CHAPTER IV

DIAGNOSIS OF INDIAN BIG FOUR AND MONOCLED COBRA SNAKEBITES IN ENVENOMED PLASMA USING SMARTPHONE-BASED DIGITAL IMAGING COLOURIMETRY METHOD

4.1 Results

4.1.1 Custom peptides (CPs) designed from major toxins of 'Big Four' venomous snakes

For each toxin, two antigenic epitopes were linked via small non-polar glycine (G) ultimately design the CPs with increased antigenic propensity. The selected toxins, their antigenic epitopes and the custom peptides derived from those epitopes have been summarised in Table 4.1.

Table 4.1. Antigenic epitopes from major toxins identified in the proteome of 'Big Four' venomous snakes of India and their antigenic propensities before and after custom modification.

Name of unique toxin	**Antigenic epitopes**	**Antigenic propensity of epitopes**	**Epitope-based synthetic peptides. Modified residues are underlined, and the peptide length is shown in parenthesis**	**Antigenic propensity of modified peptides**	**Designation of custom peptide**
Naja naja (PLA_2 toxin)	^{63}PVDDLDRCCQVHDNC^{77}	1.0496	PVDDLDRCCQVHDGGGGNACAASVCDCDRLAAICFAG (37)	1.0819	CP 1
	^{110}NACAAAVCDCDRLAAICFAG^{130}				
Daboia russelii (PLA_2 toxin)	^{40}TDRCCFVHDCCYGNLPDC^{57}	1.0453	TDRCCFVHDCCYGNLGGGGENRICECDKAAAICFR (35)	1.0612	CP 2
	^{82}ENRICECDKAAAICFR^{97}				

Echis carinatus (Echicetin toxin)	[51]EEILVDIVVS[60] [91]FFRSYEIAIRYSECFVLEKQSVFRTWVAT[119]	1.0285	EEILVDIVVSGGGFRSYEIAIRYSECFVLEKQSVFRTWVATP (42)	1.0636	CP 3
Bungarus caeruleus (Basic phospholipase A_2 beta-bungarotoxin)	[64]PIDALDRCCYVHDNCYG[80] [101]RRTIICYGAAGTCARIVCDCDRTAALCFGD[130]	1.0536	PIDALDRCCYVHDNCYGGGRRTIICYGAAGTCARIVCDCDRTAALCFGD (49)	1.0736	CP 4
Bungarus caeruleus (Basic phospholipase A_2 KPA2 toxin)	[62]PVDELDRCCYTHD[74] [108]ADTCARFLCDCDRTAAICFASA[129]	1.0547	PVDELDRCCYTHDGGGGADTCARFLCDCDRTAAICFASA (39)	1.0591	CP 5

The KLH-conjugated CPs were used as antigens to raise polyclonal antibodies in rabbits, and then the antibodies were affinity purified to obtain the toxin-specific polyclonal antibodies (PAbs). The rabbit antisera analysed by ELISA showed the presence of a high titre of CP-specific antibodies (Fig. 4.1a-e).

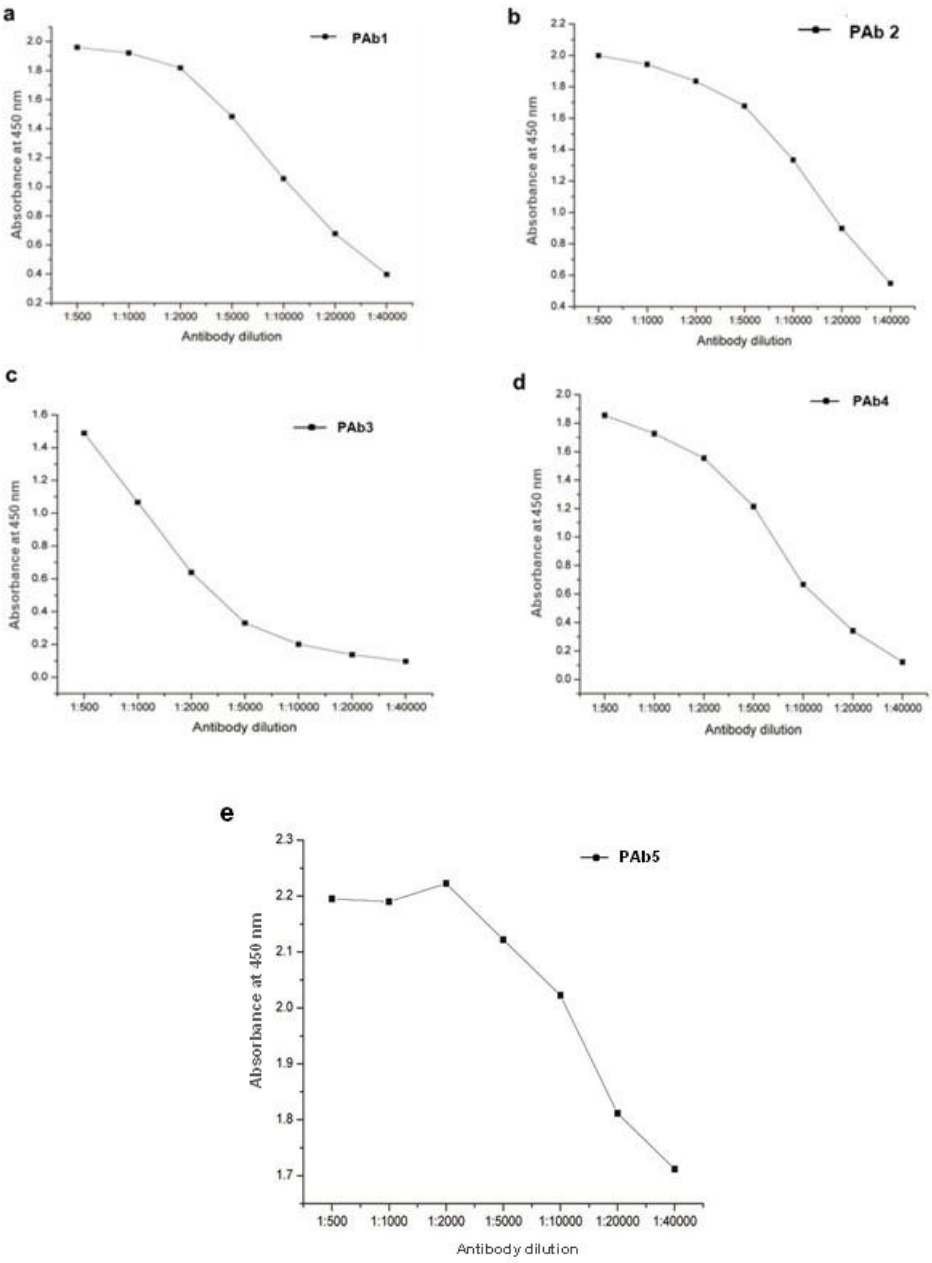

Fig. 4.1 Determination of titer of purified antibody by ELISA: **(a)** PAb1, **(b)** PAb 2, **(c)** PAb 3, **(d)** PAb 4 and **(e)** PAb 5.

4.1.1.1 Dot blot study demonstrated the ability of PAbs to recognise CPs

The PAbs showed their ability to recognise the CPs with some cross-reactivity among them under identical experimental conditions (Fig. 4.1f-k)

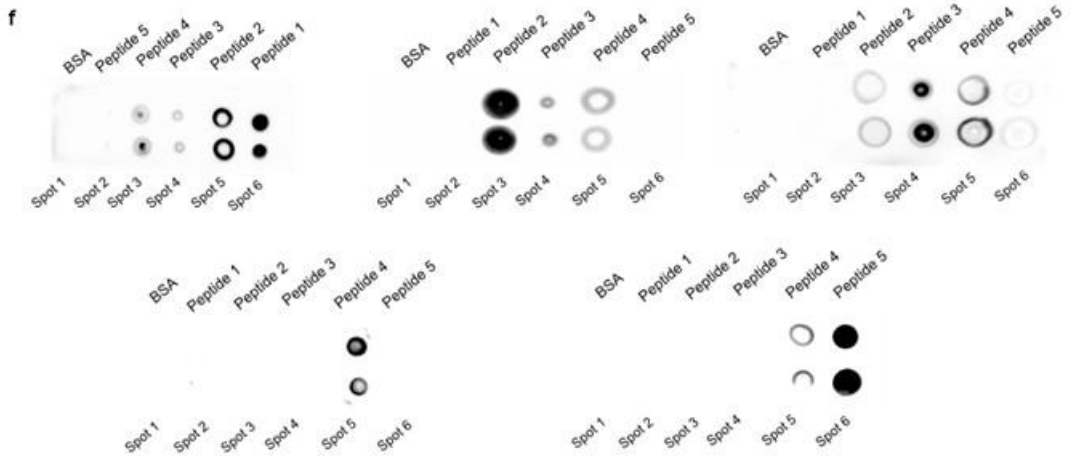
f
BSA
Peptide 5
Peptide 4
Peptide 3
Peptide 2
Peptide 1
Spot 1
Spot 2
Spot 3
Spot 4
Spot 5
Spot 6

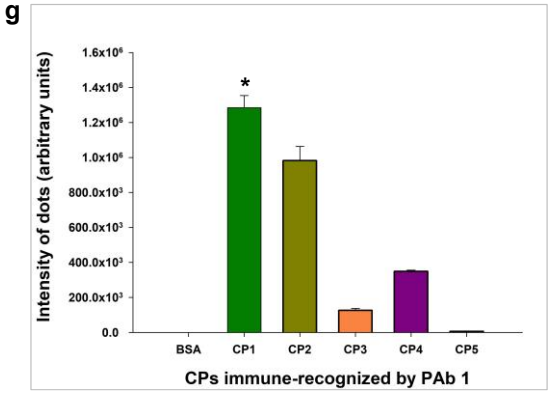
g
Intensity of dots (arbitrary units)
1.6x10⁶
1.4x10⁶
1.2x10⁶
1.0x10⁶
800.0x10³
600.0x10³
400.0x10³
200.0x10³
0.0
*
BSA
CP1
CP2
CP3
CP4
CP5
CPs immune-recognized by PAb 1

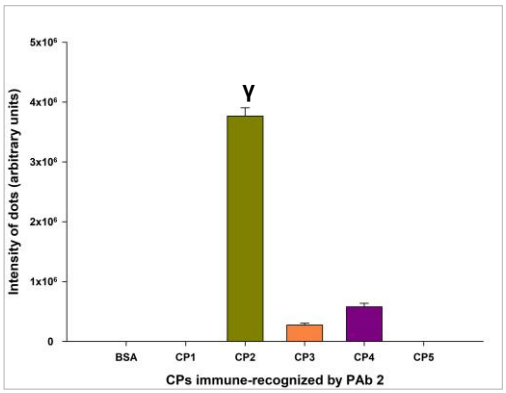
h
Intensity of dots (arbitrary units)
5x10⁶
4x10⁶
3x10⁶
2x10⁶
1x10⁶
0
γ
BSA
CP1
CP2
CP3
CP4
CP5
CPs immune-recognized by PAb 2

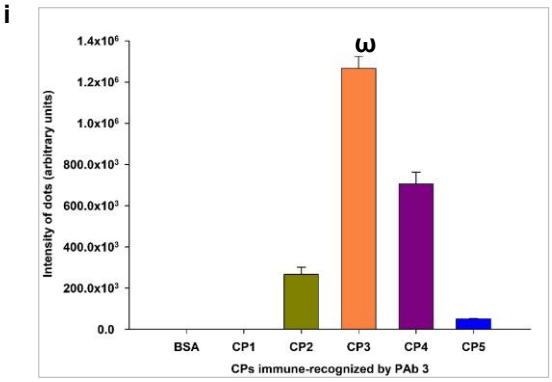
i
Intensity of dots (arbitrary units)
1.4x10⁶
1.2x10⁶
1.0x10⁶
800.0x10³
600.0x10³
400.0x10³
200.0x10³
0.0
ω
BSA
CP1
CP2
CP3
CP4
CP5
CPs immune-recognized by PAb 3

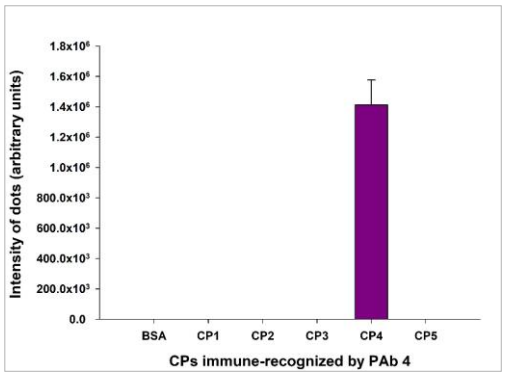
j
Intensity of dots (arbitrary units)
1.8x10⁶
1.6x10⁶
1.4x10⁶
1.2x10⁶
1.0x10⁶
800.0x10³
600.0x10³
400.0x10³
200.0x10³
0.0
BSA
CP1
CP2
CP3
CP4
CP5
CPs immune-recognized by PAb 4

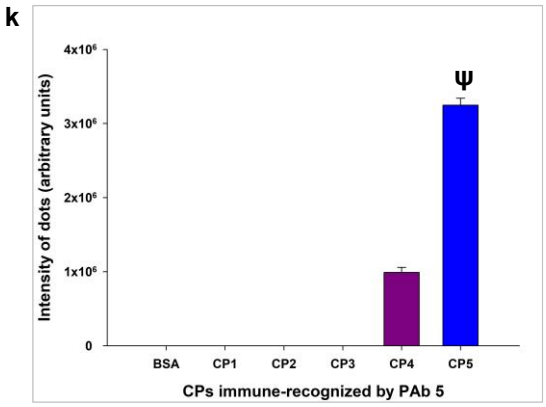

Fig. 4.1 (f) Dot blot assay to determine the immune-recognition of individual PAbs towards the corresponding CPs. Dot blot intensities of immune recognition demonstrated by the individual PAbs towards the CPs are depicted as: **(g)** PAb 1 demonstrated cross-reactivity towards CP 2-5. Significance of difference in recognition of PAb 1 towards CP 2, CP 3, CP 4 and CP 5 compared to CP 1, *$p<0.05$. **(h)** PAb 2 demonstrated some cross-reactivity towards CP 3 and CP 4. Significance of difference in recognition of PAb 2 towards CP 3 and CP 4 compared to CP 2, $^{\S}p<0.05$. **(i)** PAb 3 demonstrated cross-reactivity towards CP 2, CP 4 and CP 5. Significance of difference in recognition of PAb 3 towards CP 2, CP 4 and CP 5 compared to CP 3, $^{\omega}p<0.05$. **(j)** PAb 4 demonstrated specificity towards CP 4. **(k)** PAb 5 demonstrated cross-reactivity towards CP4. Significance of difference in recognition of PAb 5 towards CP 4 compared to CP 5, $^{\Psi}p<0.05$.

4.1.1.2 Protein-protein BLAST analysis shows the similarity of CP and *Naja kaouthia* PLA_2

The protein BLAST performed with the CP 1 and CP 4 sequences demonstrated about 90% sequence identity with the PLA_2 of *N. kaouthia* venom (Fig. 4.1 l,m).

(l)

```
CLUSTAL O(1.2.4) multiple sequence alignment


peptide                 PIDALDRCCYVHDNCYGGGRR------------------TIICYGAAGTCARIVCDCDRT    42
pir|PSNJ3K|:36-102      PVDDLDRCCQVHDNCYDEAEKISGCWPYFKTYSYESCQGTLTCKGGNNACAAAVCDCDRL    60
                        *:* ***** ******. ..:                  *: * *. .:**  ******

peptide                 AALCFGD 49
pir|PSNJ3K|:36-102      AAICFAG 67
                        **:**..
```

(m)

```
CLUSTAL O(1.2.4) multiple sequence alignment


peptide                 PVDDLDRCCQVHDG-----------------------------GGGNACAASVCDCDRL    30
pir|PSNJ3K|:36-102      PVDDLDRCCQVHDNCYDEAEKISGCWPYFKTYSYESCQGTLTCKGGNNACAAAVCDCDRL    60
                        *************.                              **.*****:*******

peptide                 AAICFAG 37
pir|PSNJ3K|:36-102      AAICFAG 67
                        *******
```

Fig. 4.1 (l) Multiple sequence alignment of CP 1 and *N. kaouthia* PLA_2 obtained after BLASTp analysis of CP 1 sequence at NCBI BLAST (https://blast.ncbi.nlm.nih.gov/) searches. **(m)** Multiple sequence alignment of CP 4 and *N. kaouthia* PLA_2 was obtained after BLASTp analysis of CP 4 sequence at NCBI BLAST searches.

4.1.2 Immunoassays and spectrofluorometric analysis exhibit superior immune recognition of FPAb towards Indian snake venoms as compared to commercial PAV (*in vitro*)

The dot blot assay conducted to assess the interaction between the secondary antibody and the capture antibody, excluding the antigen, revealed that the secondary antibody (anti-rabbit IgG-HRP/anti-horse IgG-HRP) exhibited diminished immune recognition of the capture antibody (Fig. 4.2a, b); these blots will hereafter be referred to as controls without antigen. The secondary antibody may have an affinity for the Fc region of the primary antibody. Due to non-directed immobilization, fewer Fc regions may become available while depositing the primary antibody onto the PVDF membrane.

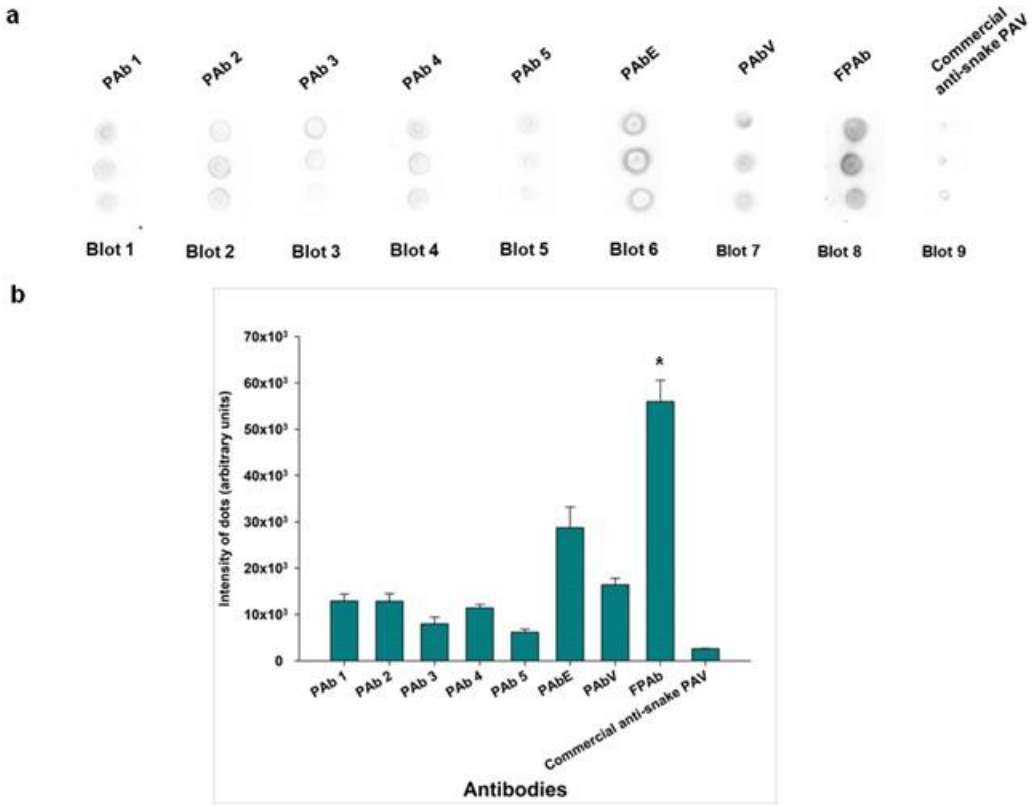

Fig. 4.2 (a) Dot blot assay to determine immune-recognition of PAbs (individual PAb 1, 2, 3, 4, 5, PAbE, PAbV and FPAb) using anti-rabbit IgG-HRP and commercial anti-snake PAV using anti-horse IgG-HRP; **(b)** Dot intensities of the immune-recognition demonstrated by the secondary antibodies as stated in (a). Significance of difference immune-recognition of FPAb by anti-rabbit IgG-HRP with respect to immune recognition of individual PAbs, PAbE, PAbV by anti-rabbit IgG-HRP and commercial PAV by anti-horse IgG-HRP, *$p<0.05$. Error bars indicate mean ± SD (n=3).

Moreover, normalizing the dot intensities against the control (excluding antigen intensities), the study revealed the enhanced in vitro immune detection of the 'Big Four' snake venoms by FPAb in comparison to the identification by the individual PAbs, PAbE, and PAbV (Fig. 4.2c, d).

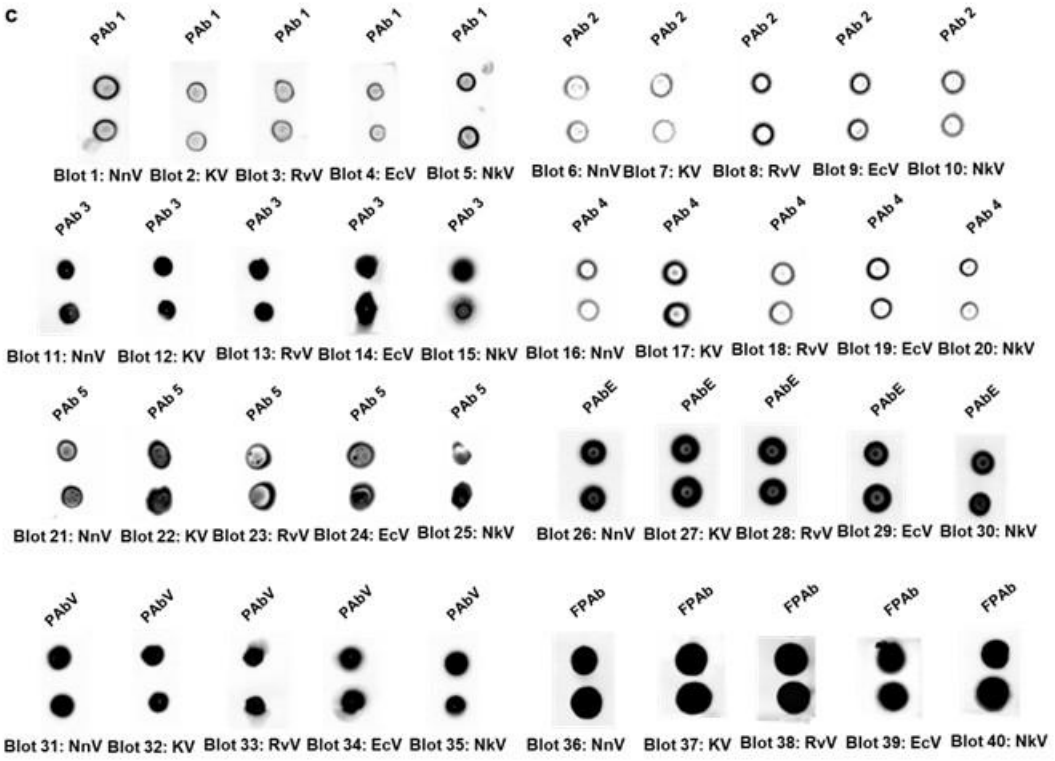

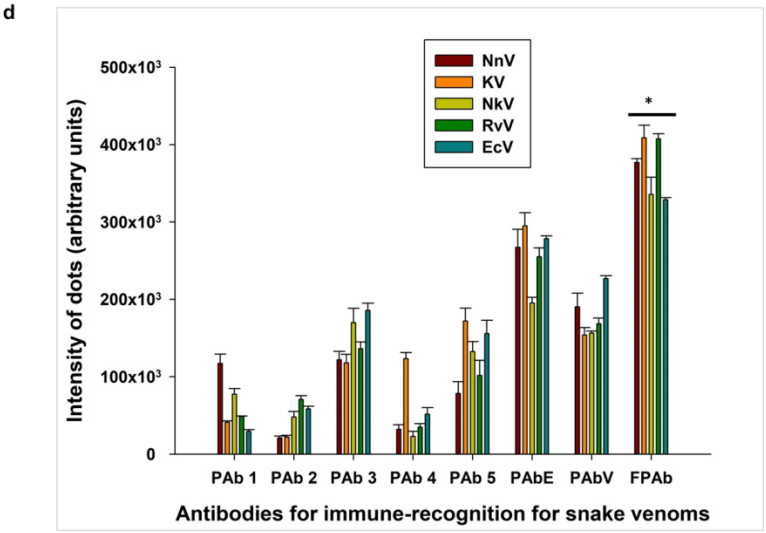

Fig. 4.2 (c) Dot blot assay to determine immune-recognition of PAbs (individual PAb 1, 2, 3, 4, 5, PAbE, PAbV and FPAb) towards NnV, KV, RvV, EcV, and NkV (1 pg/µL)**, (d)** Dot intensities of the immune-recognition of NnV, KV, RvV, EcV, and NkV by individual PAbs, PAbE, PAbV and FPAb. Significance of difference in immune-recognition of NnV, KV, RvV, EcV, and NkV by PAb 1,2,3,4, 5, PAbE and PAbV compared to immune-recognition by FPAb *$p<0.05$. Error bars indicate mean ± SD (n=3).

After normalizing the dot intensities against the control (without antigen intensities), the dot blotting with snake venom spiked rat plasma as antigen exhibited the superior immune cross-reactivity of FPAb towards venom-spiked rat plasma compared to commercial anti-snake PAV under identical experimental conditions (Fig. 4.2e, f). The FPAb/commercial anti-snake PAV did not demonstrate any cross-reactivity towards *Mesobuthus tamulus* venom-spiked rat plasma.

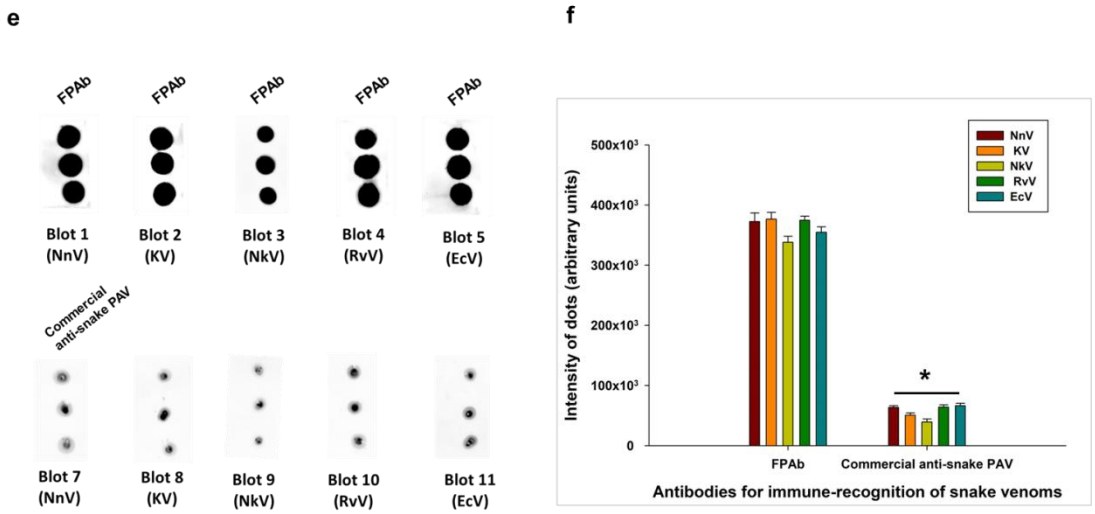

Fig. 4.2 (e) Dot blot assay to determine the immune recognition of NnV, KV, NkV, RvV, and EcV (1 pg/µL) spiked rat plasma against FPAb and commercial anti-snake PAV. **(f)** Image analyses of the intensities of the blots were performed using ImageJ software. Significance of difference of FPAb compared to commercial anti-snake PAV *$p<0.05$. Error bars indicate mean ± SD (n=3).

Western blotting analysis demonstrated the greater immune recognition of the 'Big Four' snake venoms and NkV by FPAb, compared to the immune recognition by commercial anti-snake PAV (Fig. 4.2g-i).

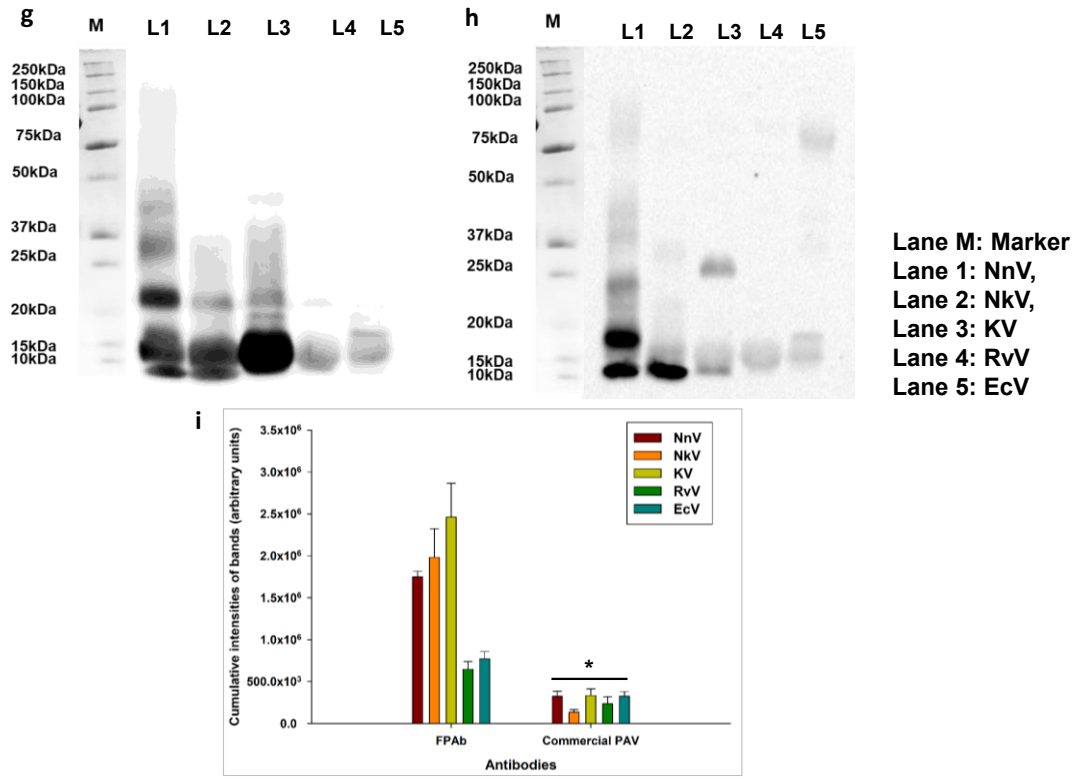

Fig. 4.2 (g) Western blot analysis to determine the immune recognition of NnV, NkV, KV, RvV and EcV against FPAb. Lane 1 represents the immunoblot of NnV, Lane 2 represents the immunoblot of NkV, Lane 3 represents the immunoblot of KV, Lane 4 represents the immunoblot of RvV, Lane 5 represents the immunoblot of EcV, and Lane M denotes the marker. Immunoblot detected by HRP conjugated anti-rabbit IgG. **(h)** Western blot analysis to determine the immune recognition of NnV, NkV, KV, RvV and EcV against commercial anti-snake PAV. Lane 1 represents the immunoblot of NnV, Lane 2 represents the immunoblot of NkV, Lane 3 represents the immunoblot of KV, Lane 4 represents the immunoblot of RvV, Lane 5 represents the immunoblot of EcV, and Lane M denotes the marker. Immunoblot detected by HRP conjugated anti-horse IgG. **(i)** Densitometry analyses of the blot intensities of NnV, NkV, KV, RvV, and EcV detected by FPAb and commercial anti-snake PAV. Significance of difference in recognition of the snake venoms by FPAb compared to recognition by commercial anti-snake PAV *$p<0.05$. Error bars indicate mean ± SD (n=3).

The K_D values of the interaction between the snake venoms and FPAb/commercial anti-snake PAV were determined in the mg protein content of FPAb or commercial anti-snake PAV/mL [1]. The results elucidated the higher affinity of FPAb towards venom antigens as compared to commercial anti-snake PAV (less K_D

value of FPAb compared to anti-snake PAV against the same venom sample) (Fig. 4.2j-n).

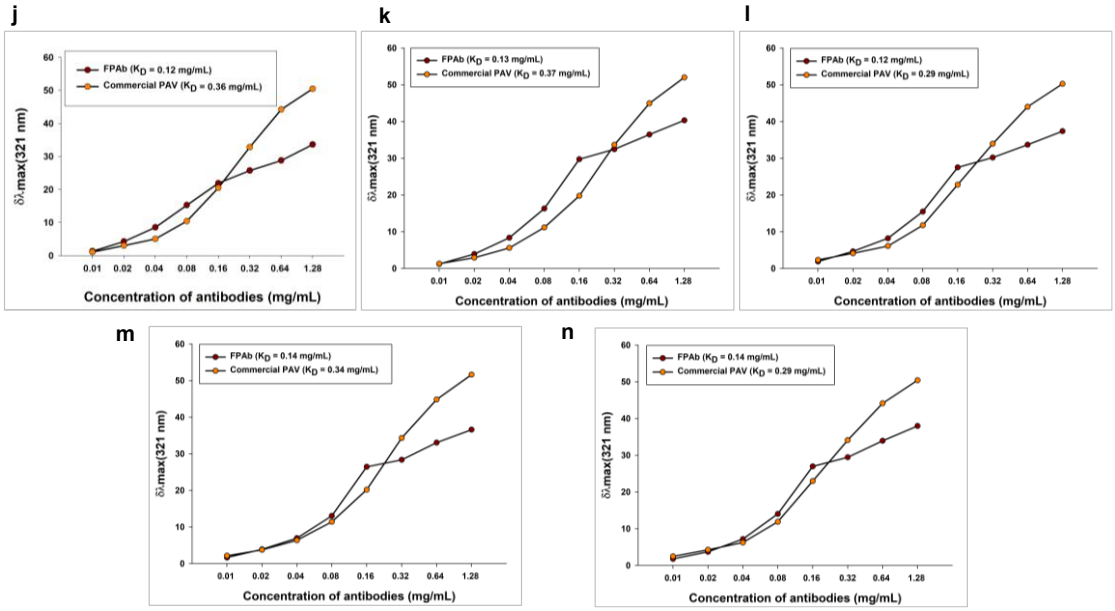

Fig. 4.2 Data showing spectrofluorometric interaction between the snake venoms, FPAb and commercial anti-snake PAV. The interactions between the fixed concentration of each venom and varying concentrations of FPAb and commercial anti-snake PAV have been represented in a one-site specific binding curve showing the change in maximum fluorescence intensity (λ_{max}) of venom-antibody binding. **(j)** Interaction of NnV with FPAb and commercial anti-snake PAV, **(k)** Interaction of KV with FPAb and commercial anti-snake PAV, **(l)** Interaction of NkV with FPAb and commercial anti-snake PAV, **(m)** Interaction of RvV with FPAb and commercial anti-snake PAV, and **(n)** Interaction of EcV with FPAb and commercial anti-snake PAV. The graphs were plotted using GraphPad Prism 5.0 software and demonstrate the mean of five scans.

4.1.3 The FPAb demonstrated better immune-recognition towards the Indian snake venoms as compared to commercial anti-snake PAV in envenomed rat plasma

Dot blot analysis depicted the time-dependent immune recognition of the snake venoms by FPAb in the plasma of subcutaneously envenomed Wistar rats. In NnV envenomed rats (group 2), no significant difference was found in the venom recognition by FPAb between 60- and 120-min post-injection; however, a slight decline in immune recognition was observed at 240 min (Fig. 4.3a, b). Maximum venom recognition of KV

in group 3 rats' plasma by FPAb was observed at 60 min and 120 min post-injection, with a decline of immune recognition at 240 min (Fig. 4.3c, d). The FPAb showed the highest detection of NkV in plasma (group 4) at 60 min post-injection; however, the immune recognition of FPAb demonstrated a gradual decline at 120 min and 240 min post-injection NkV plasma (Fig. 4.3e, f).

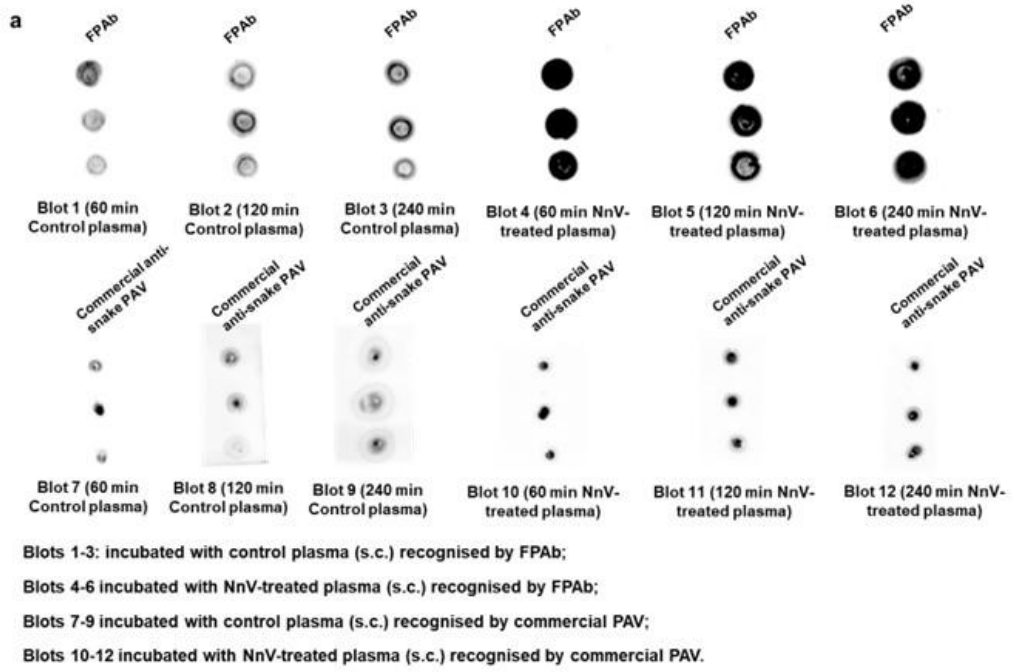

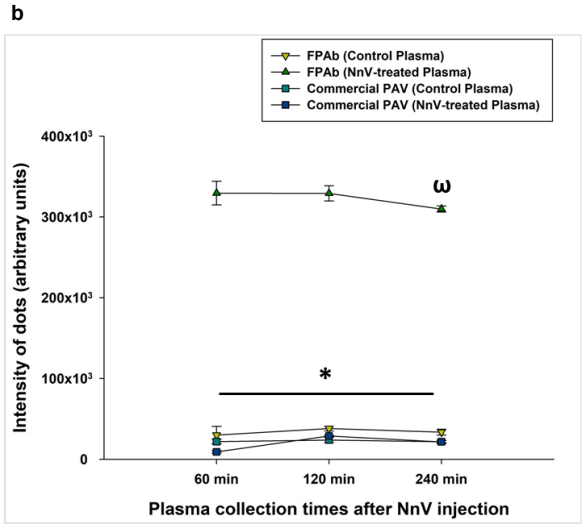

Fig. 4.3 (a) Dot blot assay to determine immune-recognition of NnV in the plasma of the group 1 and 2 rats by FPAb and commercial anti-snake PAV when the blood was collected at 60 min, 120 min, and 240 min post-injection (s.c.). Blots 1-3 incubated with control plasma (s.c.) collected after 60 min, 120 min, and 240 min recognised by FPAb;

Blots 4-6 incubated with NnV -treated plasma (s.c.) collected after 60 min, 120 min, and 240 min recognised by FPAb; Blots 7-9 incubated with control plasma (s.c.) collected after 60 min, 120 min, and 240 min recognised by commercial anti-snake PAV; Blots 10-12 incubated with NnV-treated plasma (s.c.) collected after 60 min, 120 min, and 240 min recognised by commercial anti-snake PAV. **(b)** Dot intensities of NnV-envenomed rats' plasma immune-recognised by FPAb and commercial anti-snake PAV were analysed using ImageJ. Significance of difference in recognition of plasma collected from NnV-envenomed rats (s.c.) at 60 min and 120 min compared to plasma collected at 240 min, $^{\omega}p<0.05$; recognition of plasma collected at 60 min, 120 min and 240 min by FPAb compared to recognition by commercial anti-snake PAV, $*p<0.05$. Error bars indicate mean ± SD (n=3).

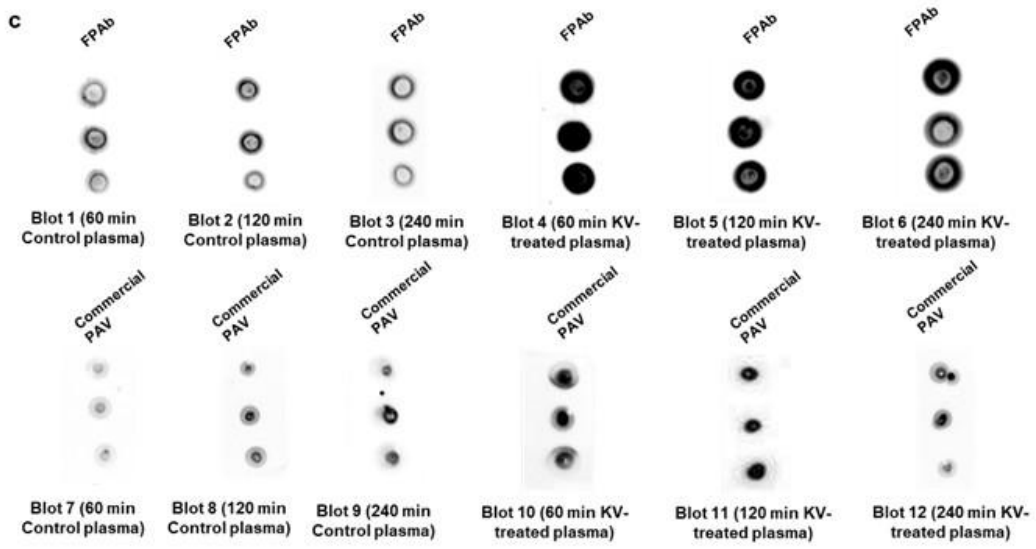

Blots 1-3: incubated with control plasma (s.c.) recognised by FPAb;

Blots 4-6 incubated with KV-treated plasma (s.c.) recognised by FPAb;

Blots 7-9 incubated with control plasma (s.c.) recognised by commercial PAV;

Blots 10-12 incubated with KV-treated plasma (s.c.) recognised by commercial PAV.

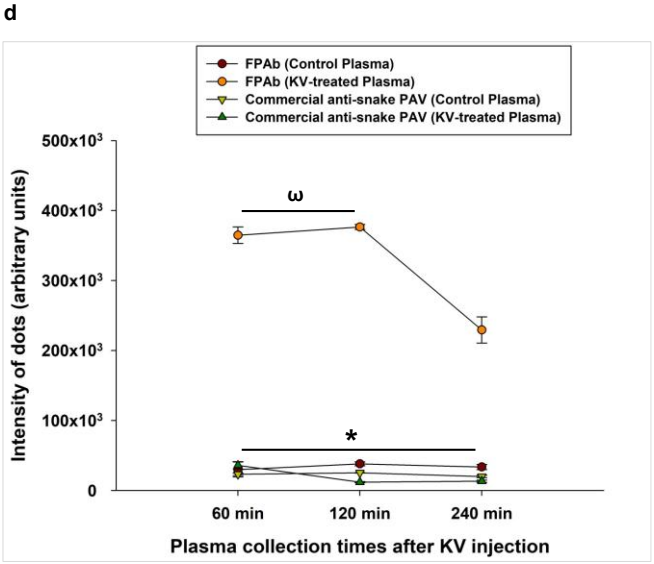

Fig. 4.3 (c) Dot blot assay to determine immune-recognition of KV in the plasma of the group 1 and 3 rats by FPAb and commercial anti-snake PAV when the blood was collected at 60 min, 120 min, and 240 min post-injection (s.c.). Blots 1-3 incubated with control plasma (s.c.) collected after 60 min, 120 min, and 240 min recognised by FPAb; Blots 4-6 incubated with KV-treated plasma (s.c.) collected after 60 min, 120 min, and 240 min recognised by FPAb; Blots 7-9 incubated with control plasma (s.c.) collected after 60 min, 120 min, and 240 min recognised by commercial anti-snake PAV; Blots 10-12 incubated with KV-treated plasma (s.c.) collected after 60 min, 120 min, and 240 min recognised by commercial anti-snake PAV. **(d)** Dot intensities of KV-envenomed rats' plasma immune-recognised by FPAb and commercial anti-snake PAV were analysed using ImageJ. Significance of difference in recognition of plasma collected from KV-envenomed rats (s.c.) at 240 min compared to plasma collected at 60 min and 120 min, $^{\omega}p<0.05$; recognition of plasma collected at 60 min, 120 min and 240 min by FPAb compared to recognition by commercial anti-snake PAV, $*p<0.05$. Error bars indicate mean ± SD (n=3).

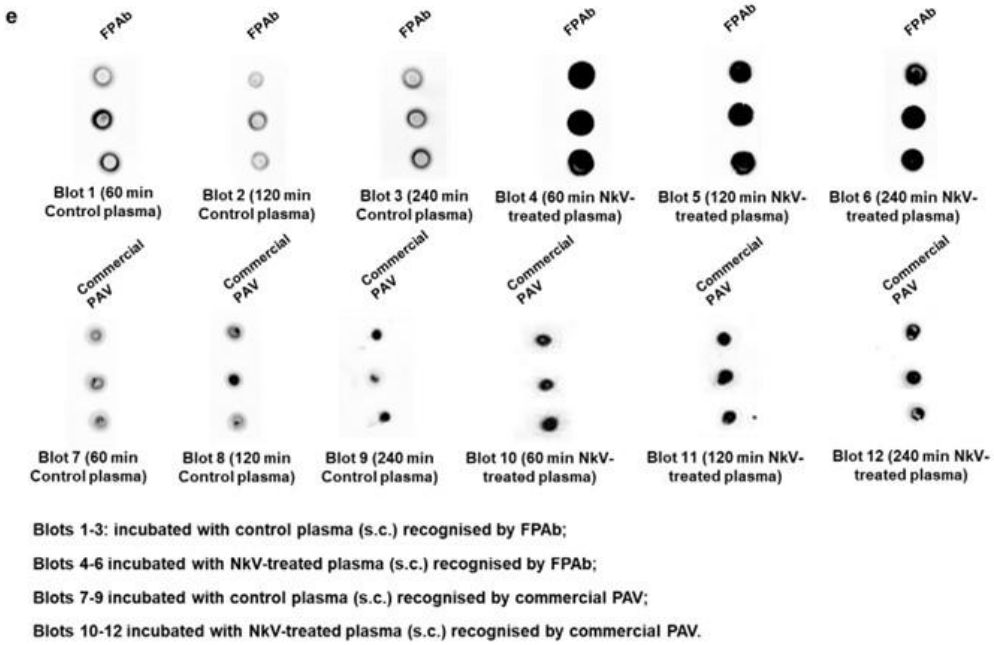

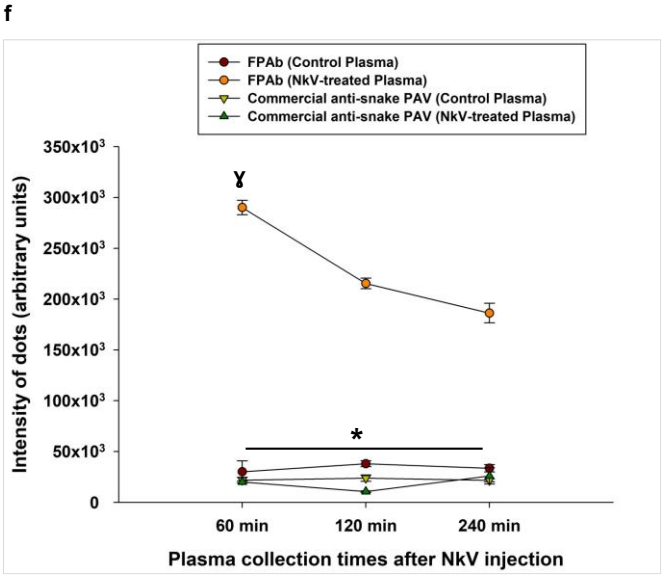

Fig. 4.3 (e) Dot blot assay to determine immune-recognition of NkV in the plasma of the group 1 and 6 rats by FPAb and commercial anti-snake PAV when the blood was collected at 60 min, 120 min, and 240 min post-injection (s.c.). Blots 1-3 incubated with control plasma (s.c.) collected after 60 min, 120 min, and 240 min recognised by FPAb; Blots 4-6 incubated with NkV-treated plasma (s.c.) collected after 60 min, 120 min, and 240 min recognised by FPAb; Blots 7-9 incubated with control plasma (s.c.) collected after 60 min, 120 min, and 240 min recognised by commercial anti-snake PAV; Blots 10-12 incubated with NkV-treated plasma (s.c.) collected after 60 min, 120 min, and

240 min recognised by commercial anti-snake PAV. **(f)** Dot intensities of NkV-envenomed rats' plasma immune-recognised by FPAb and commercial anti-snake PAV were analysed using ImageJ. Significance of difference in recognition of plasma collected from NkV-envenomed rats (s.c.) at 120 min and 240 min compared to plasma collected at 60 min, $^{\gamma}p<0.05$; recognition of plasma collected at 60 min, 120 min and 240 min by FPAb compared to recognition by commercial anti-snake PAV, $*p<0.05$. Error bars indicate mean ± SD (n=3).

For the rats injected with RvV subcutaneously (group 5), the maximum RvV recognition was observed at 60 min and 120 min post-injection, and the recognition declined significantly at 240 min (Fig. 4.3 g,h). The highest EcV recognition (group 6) was observed between 60 and 120 min post-injection, and after that, a sharp decline in the intensity of recognition was observed (Fig. 4.3 i,j). However, the intensity of recognition of venom from the Viperidae family of snakes was higher ($p \leq 0.01$) than the Elapidae family of snakes. Notably, since the antibodies constituting the FPAb were raised against antigenic peptides synthesised using the toxins of the 'Big Four' venomous snakes of India, it may have a lower affinity towards NkV; therefore, their detection in plasma may be lesser than the 'Big Four' snake venoms.

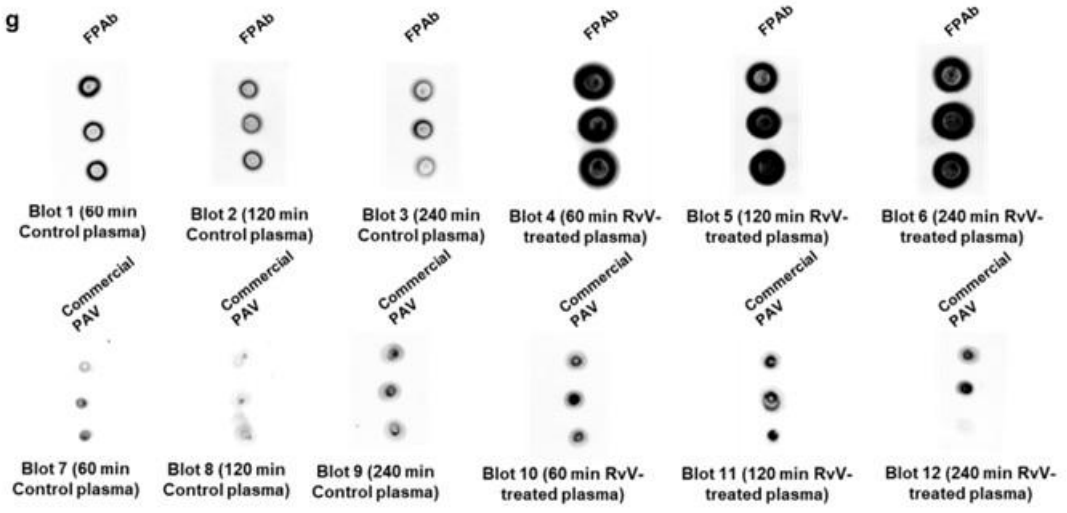

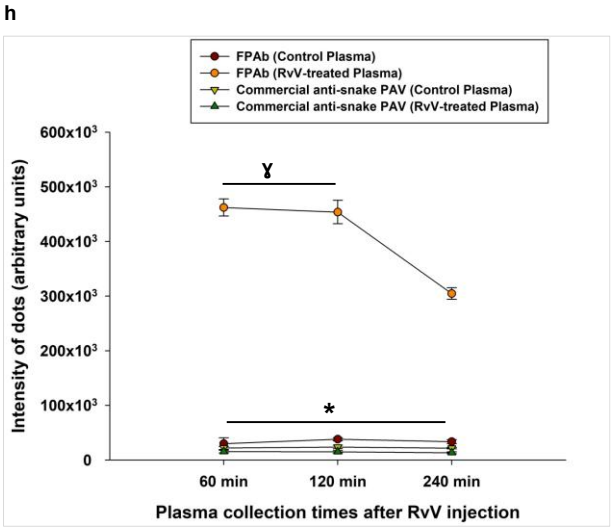

Fig. 4.3 (g) Dot blot assay to determine immune-recognition of RvV in the plasma of the group 1 and 4 rats by FPAb and commercial anti-snake PAV when the blood was collected at 60 min, 120 min, and 240 min post-injection (s.c.). Blots 1-3 incubated with control plasma (s.c.) collected after 60 min, 120 min, and 240 min recognised by FPAb; Blots 4-6 incubated with RvV-treated plasma (s.c.) collected after 60 min, 120 min, and 240 min recognised by FPAb; Blots 7-9 incubated with control plasma (s.c.) collected after 60 min, 120 min, and 240 min recognised by commercial anti-snake PAV; Blots 10-12 incubated with RvV-treated plasma (s.c.) collected after 60 min, 120 min, and 240 min recognised by commercial anti-snake PAV. **(h)** Dot intensities of RvV-envenomed rats' plasma immune-recognised by FPAb and commercial anti-snake PAV were analysed using ImageJ. Significance of difference in recognition of plasma collected from RvV-envenomed rats (s.c.) at 240 min compared to plasma collected at 60 min and 120 min, $^{\gamma}p<0.05$; recognition of plasma collected at 60 min, 120 min and 240 min by FPAb compared to recognition by commercial anti-snake PAV, $*p<0.05$. Error bars indicate mean ± SD (n=3).

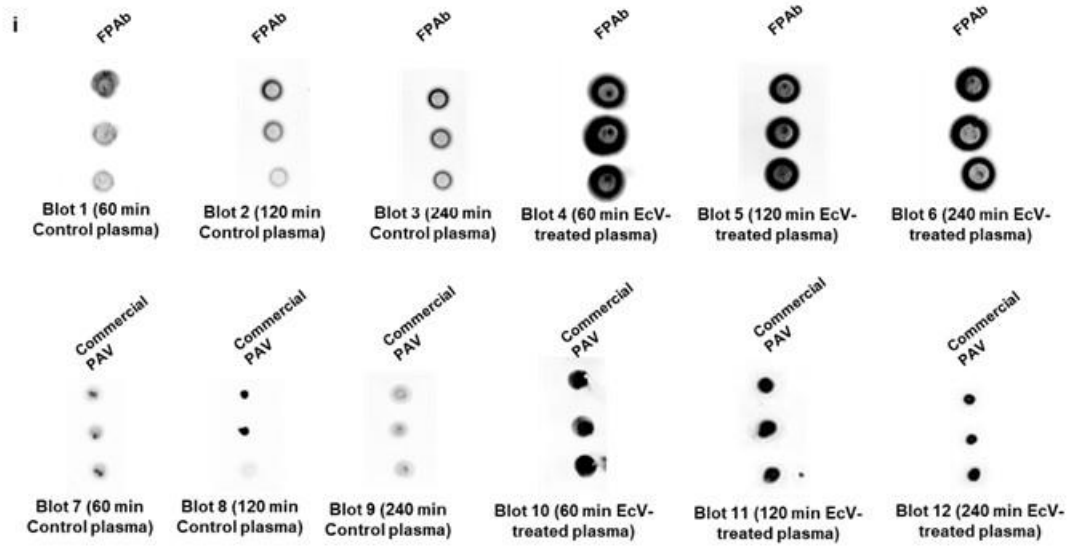

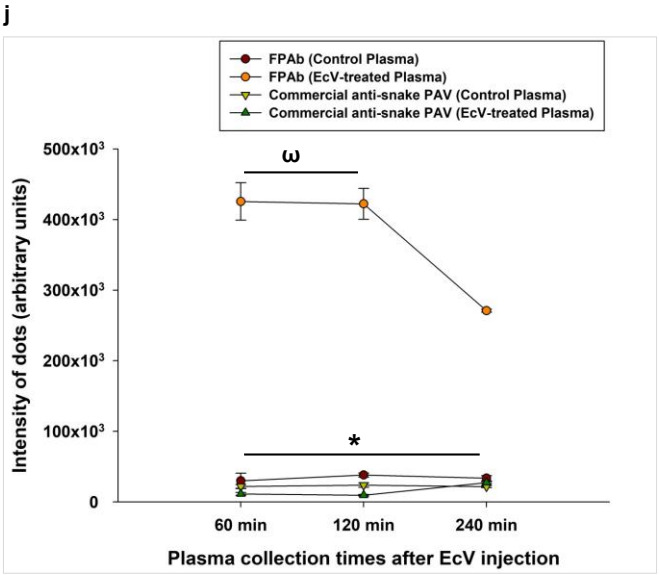

Fig. 4.3 (i) Dot blot assay to determine immune-recognition of EcV in the plasma of the group 1 and 5 rats by FPAb and commercial anti-snake PAV when the blood was collected at 60 min, 120 min, and 240 min post-injection (s.c.). Blots 1-3 incubated with control plasma (s.c.) collected after 60 min, 120 min, and 240 min recognised by FPAb; Blots 4-6 incubated with EcV-treated plasma (s.c.) collected after 60 min, 120 min, and 240 min recognised by FPAb; Blots 7-9 incubated with control plasma (s.c.) collected after 60 min, 120 min, and 240 min recognised by commercial anti-snake PAV; Blots

10-12 incubated with EcV-treated plasma (s.c.) collected after 60 min, 120 min, and 240 min recognised by commercial anti-snake PAV. **(j)** Dot intensities of EcV-envenomed rats' plasma immune-recognised by FPAb and commercial anti-snake PAV were analysed using ImageJ. Significance of difference in recognition of plasma collected from EcV-envenomed rats (s.c.) at 240 min compared to plasma collected at 60 min and 120 min, $^{\omega}p<0.05$; recognition of plasma collected at 60 min, 120 min and 240 min by FPAb compared to recognition by commercial anti-snake PAV, $*p<0.05$. Error bars indicate mean ± SD (n=3).

In all the cases, dot blot analysis demonstrated the superior immune recognition of tested snake venoms by FPAb compared to commercial anti-snake PAV raised against native toxins under identical experimental conditions (Fig. 4.3a-j).

4.1.4 Biophysical characterisation demonstrated conjugation of FPAb with AuNPs

The production of gold nanoparticles (AuNPs) using citrate reduction involves the utilisation of citrate to aid the reduction of gold (III) to gold (0), hence imposing growth limitations on the AuNPs [2-4]. The following scheme depicts the reaction during citrate reduction-based AuNP synthesis (Fig. 4.4a).

a

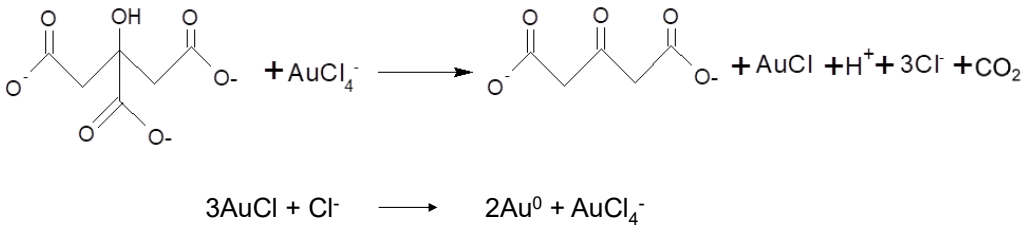

Fig. 4.4 (a) Chemical reaction sequence for citrate reduction-based AuNP synthesis.

The AuNPs synthesised by this method exhibited a wine-red colour, and their UV-Vis spectra (400-700 nm) depicted a plasmonic peak at around 527 nm. After the conjugation of FPAb to the citrate-capped AuNPs, the plasmonic peak showed a bathochromic shift to 537 nm (Fig. 4.4b).

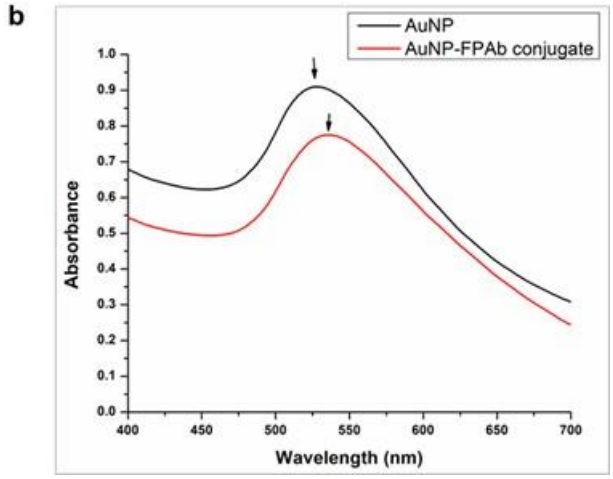

Fig. 4.4 (b) UV-Vis spectra depicting AuNP and AuNP-FPAb conjugate. The absorbance is the mean of values obtained in triplicates.

FTIR presented an infrared spectrum of AuNP with peaks at 3368 cm^{-1}, 1567 cm^{-1}, 1475 $cm^{-1,}$ and 1399 $cm^{-1,}$ characteristic of –O–H stretching, –C=O stretching, and –C–H bending, and indicate the formation of citrate-stabilised AuNPs [5]. After conjugation of FPAb to AuNP, the peaks associated with –O–H stretching and –C=O stretching disappeared, and new peaks appeared at 1622 cm^{-1} and 1532 cm^{-1} which correspond to primary amide NH_2 bending and secondary amide N‑H bending under the amide II band, respectively [5] (Fig. 4.4c).

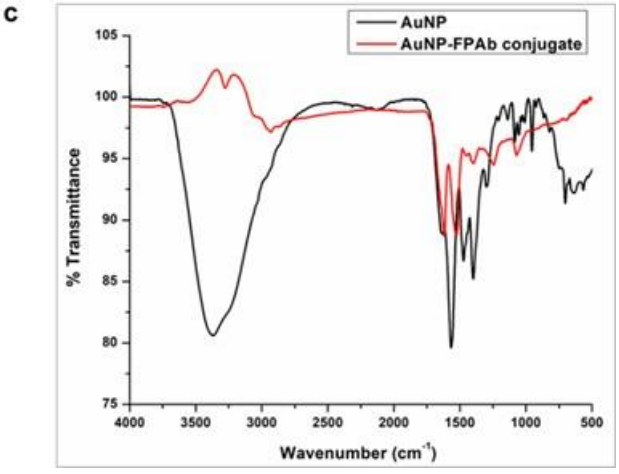

Fig. 4.4 (c) FTIR spectra of AuNP and AuNP-FPAb conjugate.

The citrate-capped AuNPs and AuNP-FPAb conjugate recorded zeta potential (mV) of −34.7 ± 0.173 mV and −26.8 ± 0.02 mV, respectively (Fig. 4.4d).

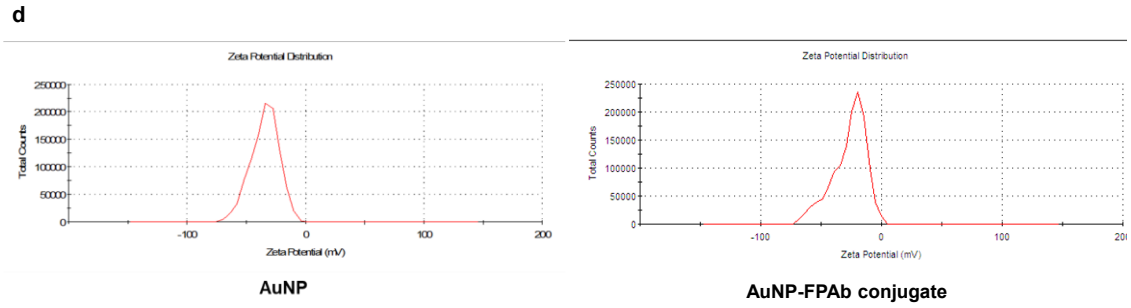

Fig. 4.4 (d) Zeta potential of AuNP and AuNP-FPAb conjugate.

The TEM analysis performed in this study showed the synthesis of monodisperse citrate-capped AuNPs, which were aggregated after conjugation to FPAb (Fig. 4.4e, f). From the images obtained, the average diameter of the AuNP and AuNP-FPAb conjugate particles was determined at 18.99 ± 0.41 nm and 37.52 ± 0.99 nm, respectively (Fig. 4.4g, h).

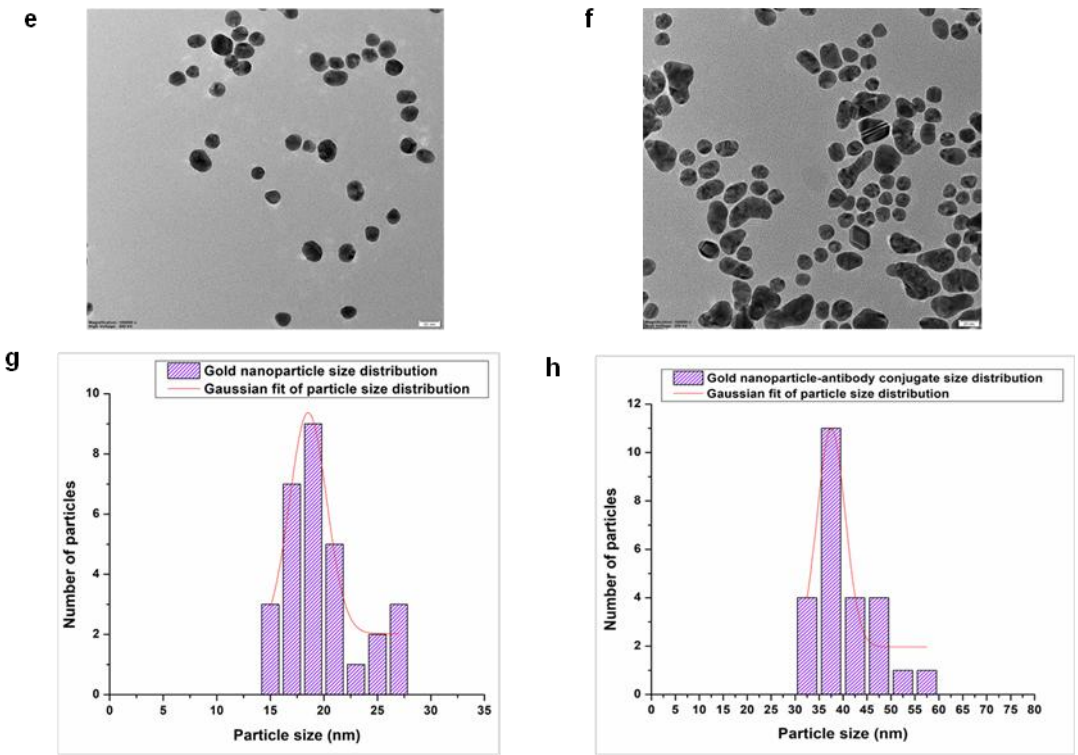

Fig. 4.4 TEM images of **(e)** AuNP and **(f)** AuNP-FPAb conjugate particle at 20 nm magnification; Histogram depicting Particle size distribution of **(g)** AuNP and **(h)** AuNP-FPAb conjugate particle in TEM images, with Gaussian function, fit using Originpro 8.5.

The AFM analysis further demonstrated the synthesis and conjugation of AuNPs performed (Fig. 4.4i, j), which depicted that the citrate-capped AuNPs and AuNP-FPAb conjugate particles measured their heights at 18.53 ± 0.26 nm and 36.21 ± 0.45 nm, respectively (Fig. 4.4k, l).

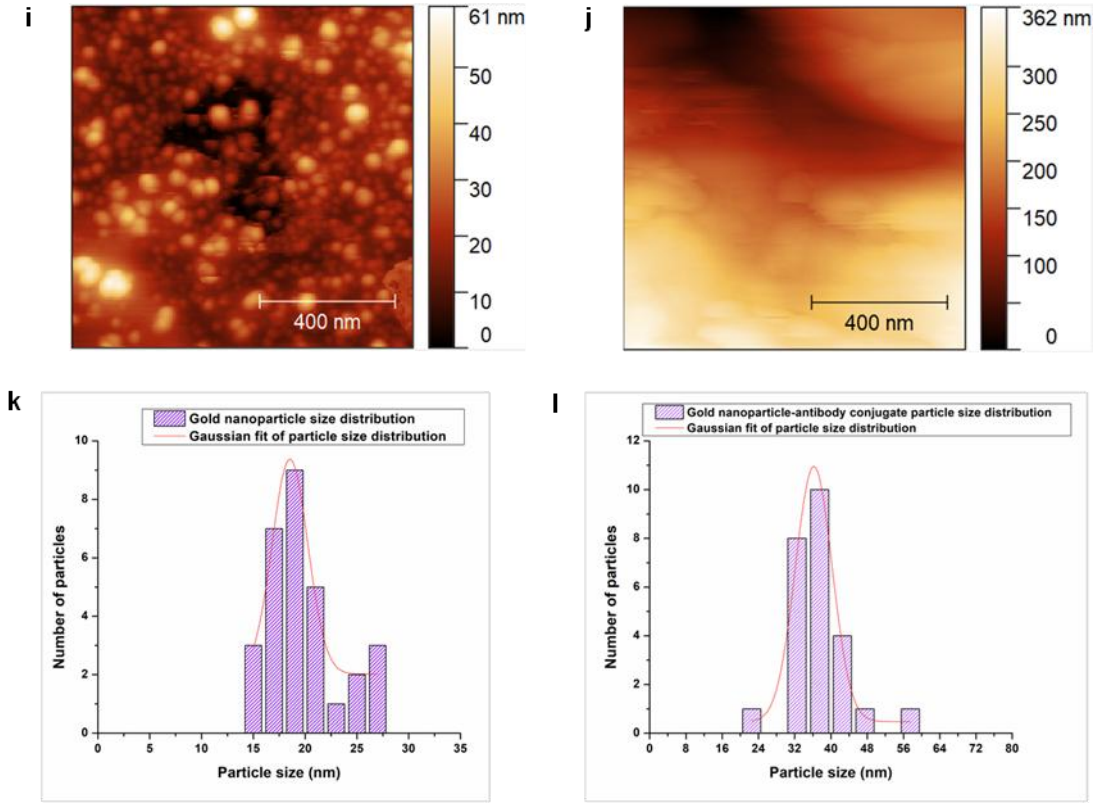

Fig. 4.4 Topographic 2D AFM images with scanned area 1000 x 1000 nm of **(i)** AuNP, **(j)** AuNP-FPAb conjugate; Histogram of height distribution of **(k)** AuNP, **(l)** AuNP-FPAb conjugate, from the topographic 2D AFM images with scanned area 1000 x 1000 nm.

The adsorption efficiency of FPAb to AuNP was determined at 59.3% (Fig. 4.4m).

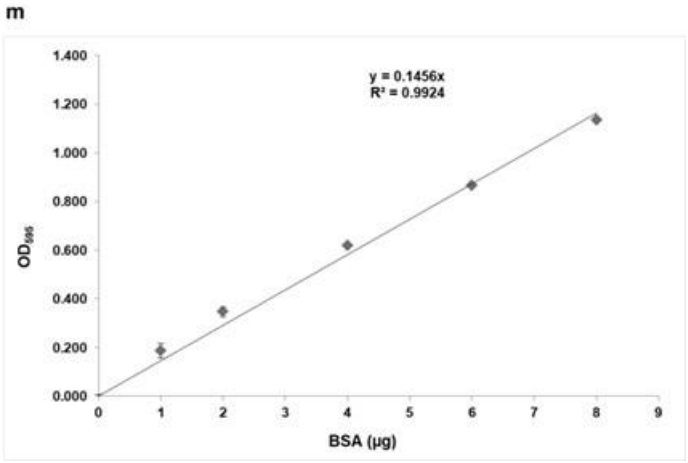

Fig. 4.4 (m) Calibration curve for estimating FPAb left in the supernatant after AuNP-conjugation. Error bars indicate mean ± SD (n=3).

4.1.5 Detection of Indian snake venoms in envenomed Wistar strain rats (*in vivo*) by AuNP-FPAb conjugate using digital image colourimetry

Snake venoms spiked in rat plasma were detected using smartphone images. From the images recorded, the average R (red), G (green), and B (blue) values were analysed using ImageJ. The RGB colour values obtained were converted to a logarithmic scale to get the colour intensity according to the Lambert-Beer law equation [6,7]:

Colour Intensity of Red (I_R) = log (R_0/R_S), ..Equation 1

Colour Intensity of Green (I_G) = log (G_0/G_S), ..Equation 2

Colour Intensity of Blue (I_B) = log (B_0/B_S), ..Equation 3

The average blank and sample colour values are R_0, G_0, B_0, R_S, G_S, and B_S, respectively.

Linear regression standard curves were prepared from the colour intensities obtained from each venom-spiked plasma (Fig. 4.5a-e). From the equations and R^2 values depicted in Fig. 4.5a-e, the blue (B) colour showed the highest linearity as compared to the red (R) and green (G) colours for all the snake venoms studied. This observation may be due to the change in colour of AuNP-FPAb conjugates from burgundy to blue upon binding with venoms.

From the equations obtained from the linear regression curves (Fig. 4.5a-e), the limit of detection (LoD) for blue colour was determined to be 330 pg/µL (NnV), 240 pg/µL (KV), 430 pg/µL (NkV), 210 pg/µL (RvV), and 620 pg/µL (EcV). The LoD was determined using the formula 3.3 σ/S, where σ is the standard deviation of the response, and S is the slope of the calibration curve.

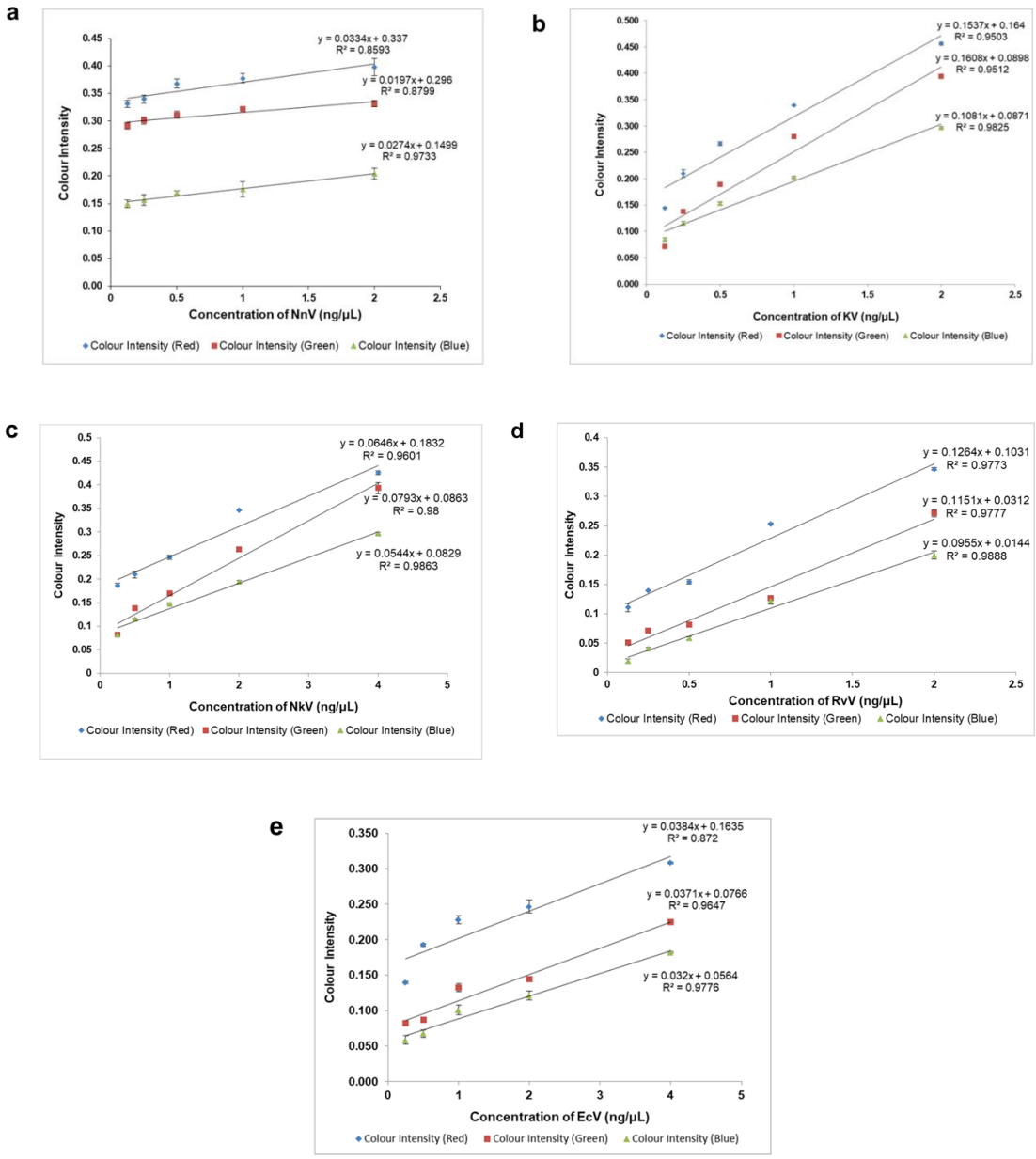

Fig. 4.5 Linear fitted plot based on the relationship between colour intensities obtained from RGB of smartphone images and different concentrations of snake venom spiked rat plasma. **(a)** NnV concentrations 0.125-2 ng/µL, **(b)** KV concentrations 0.125-2 ng/µL, **(c)** NkV concentrations 0.25-4 ng/µL, **(d)** RvV concentrations 0.125-2 ng/µL, **(e)** EcV concentrations 0.25-4 ng/µL. Error bars indicate mean ± SD (n=3)

The plasma samples obtained from the retro-orbital blood collected from the subcutaneously envenomed rat plasma samples were detected with AuNP-FPAbs, and the images recorded were analysed by ImageJ software (Fig. 4.5f-k). The I_B was calculated from the images of time-dependent plasma collected for all the snake venoms studied, the quantity of venom in plasma was calculated using equation 4 as shown below and the results have been summarized in Table 4.2. The alterations in colour resulting from the interaction between the envenomed plasmas and AuNP-FPAb conjugates were measured as absorbance with a UV-Vis spectrophotometer (Fig 4.5l-p). Calibration curves were systematically prepared for each of the snake venom spiked plasmas (Fig 4.5 q-z), and the resulting equations were employed to quantify the amount of snake venom detected in the envenomed plasmas (Table 4.2).

$$Quantity\ of\ venom\ in\ plasma\ calculated\ using\ IB/absorbance\ (in\ percent\ of\ venom\ found\ in\ plasma) =$$

*Quantity of venom in plasma calculated using linear regression curve of IB/absorbance (ng/µL) / Amount of venom injected in 220 g rat (total blood volume in 220 g rat assumed to be 15 mL) (ng/µL) * 100* .. Equation 4

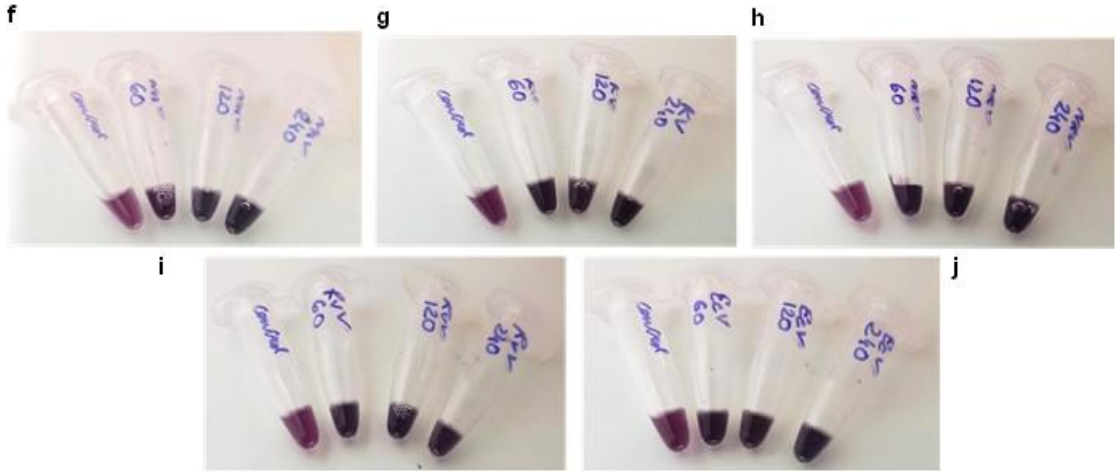

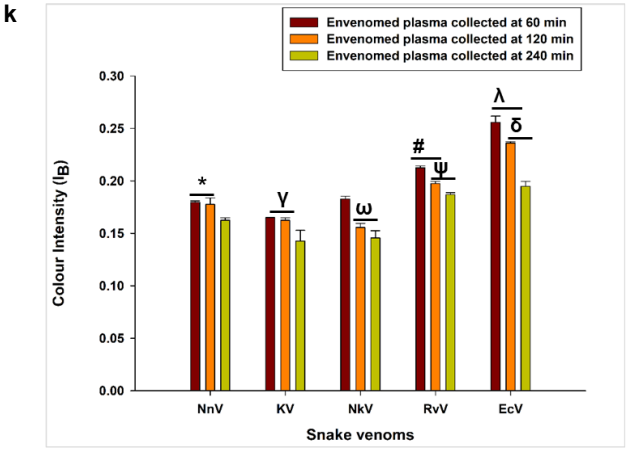

Fig. 4.5 Colour changes of AuNP-abs in the presence of control and venom-treated rat plasma. In the case of control plasma, the AuNP-ab conjugate's colour is violet-pink, while in the venom-treated plasmas, the colour changes to blue-grey due to aggregation of the AuNPs. **(f)** NnV-envenomed rat plasma collected at 60 min, 120 min and 240 min**, (g)** KV-envenomed rat plasma collected at 60 min, 120 min and 240 min, **(h)** NkV-envenomed rat plasma collected at 60 min, 120 min and 240 min, **(i)** RvV-envenomed rat plasma collected at 60 min, 120 min and 240 min, **(j)** EcV-envenomed rat plasma collected at 60 min, 120 min and 240 min, **(k)** Blue colour intensities (I_B) of all the snake venom-treated rat plasmas compared to the control plasma. Significance of difference for I_B of NnV-treated plasma collected at 60 and 120 min compared to I_B of NnV-treated plasma collected at 240 mi,n $^{*}p<0.05$; I_B of KV-treated plasma collected at 60 and 120 min compared to I_B of KV-treated plasma collected at 240 min, $^{\gamma}p<0.05$; I_B of NkV-treated plasma collected at 120 and 240 min compared to I_B of NkV-treated plasma collected at 60 min, $^{\omega}p<0.05$; I_B of RvV-treated plasma collected at 60 and 120 min compared to I_B of RvV-treated plasma collected at 240 min, $^{\#}p<0.05$; I_B of RvV-treated plasma collected at 120 and 240 min compared to I_B of RvV-treated plasma collected at 60 min, $^{\psi}p<0.05$; I_B of EcV-treated plasma collected at 60 and 120 min compared to I_B of EcV-treated plasma collected at 240 min, $^{\lambda}p<0.05$; I_B of EcV-treated plasma collected at 120 and 240 min compared to I_B of EcV-treated plasma collected at 60 min, $^{\delta}p<0.05$. Error bars indicate mean ± SD (n=3).

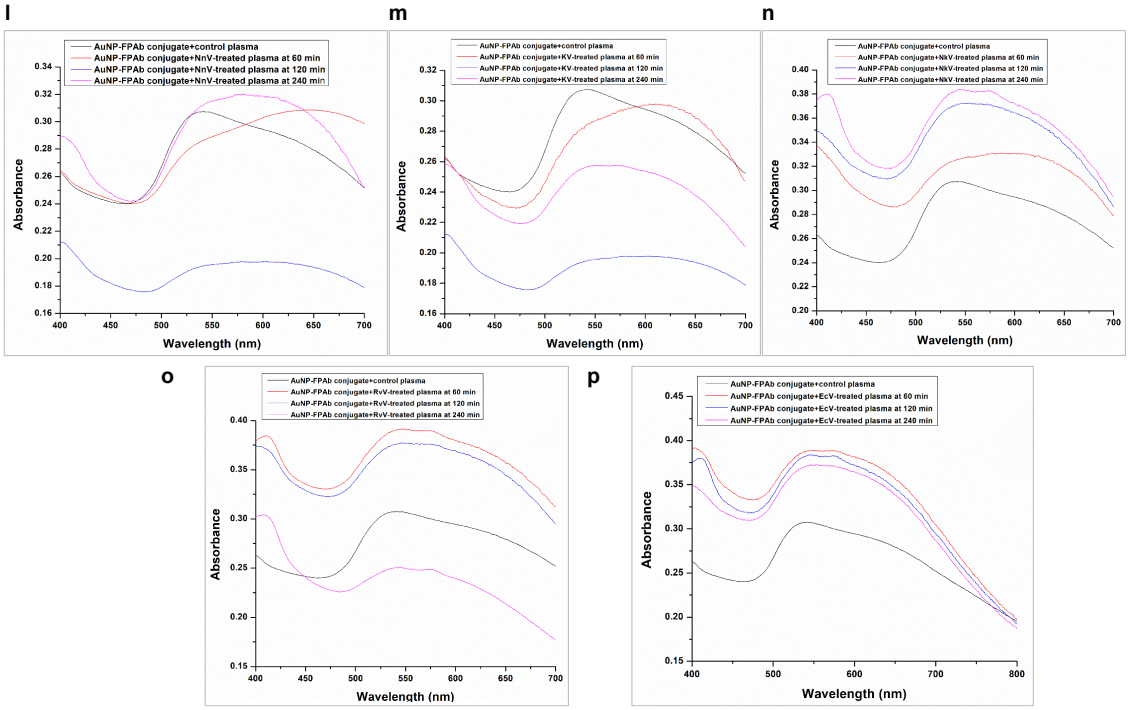

Fig 4.5 (l) Absorbance spectra of the AuNP-FPAb conjugate in the presence of control (untreated, group 1 rats) and NnV-treated plasma collected at 60 min, 120 min and 240 min post-injection (group 2 rats). The absorption maximum (λ_{max}) for Control plasma was at 537 nm. On interacting with the envenomed plasma, the λ_{max} shifted to 630 nm, 602 nm and 580 nm for NnV-treated plasma collected at 60 min, 120 min and 240 min, respectively.; **(m)** Absorbance spectra of the AuNP-FPAb conjugate in the presence of control (untreated, group 1 rats) and KV-treated plasma collected at 60 min, 120 min and 240 min post-injection (group 3 rats). The absorption maximum (λ_{max}) for Control plasma was at 537 nm. On interacting with the envenomed plasma, the λ_{max} shifted to 610 nm, 589 nm and 555 nm for KV-treated plasma collected at 60 min, 120 min and 240 min, respectively.; **(n)** Absorbance spectra of the AuNP-FPAb conjugate in the presence of control (untreated, group 1 rats) and NkV-treated plasma collected at 60 min, 120 min and 240 min post-injection (group 6 rats). The absorption maximum (λ_{max}) for Control plasma was at 537 nm. On interacting with the envenomed plasma, the λ_{max} shifted to 604 nm, 548 nm and 546 nm for NkV-treated plasma collected at 60 min, 120 min and 240 min, respectively.; **(o)** Absorbance spectra of the AuNP-FPAb conjugate in the presence of control (untreated, group 1 rats) and RvV-treated plasma collected at 60 min, 120 min and 240 min post-injection (group 4 rats). The absorption maximum (λ_{max}) for Control plasma was at 537 nm. On interacting with the envenomed plasma, the λ_{max} shifted to 548 nm, 547 nm and 543 nm for RvV-treated plasma collected at 60 min, 120

min and 240 min, respectively.; **(p)** Absorbance spectra of the AuNP-FPAb conjugate in the presence of control (untreated, group 1 rats) and EcV-treated plasma collected at 60 min, 120 min and 240 min post-injection (group 5 rats). The absorption maximum (λ_{max}) for Control plasma was at 537 nm. On interacting with the envenomed plasma, the λ_{max} shifted to 550 nm, 548 nm and 547 nm for EcV-treated plasma collected at 60 min, 120 min and 240 min, respectively.

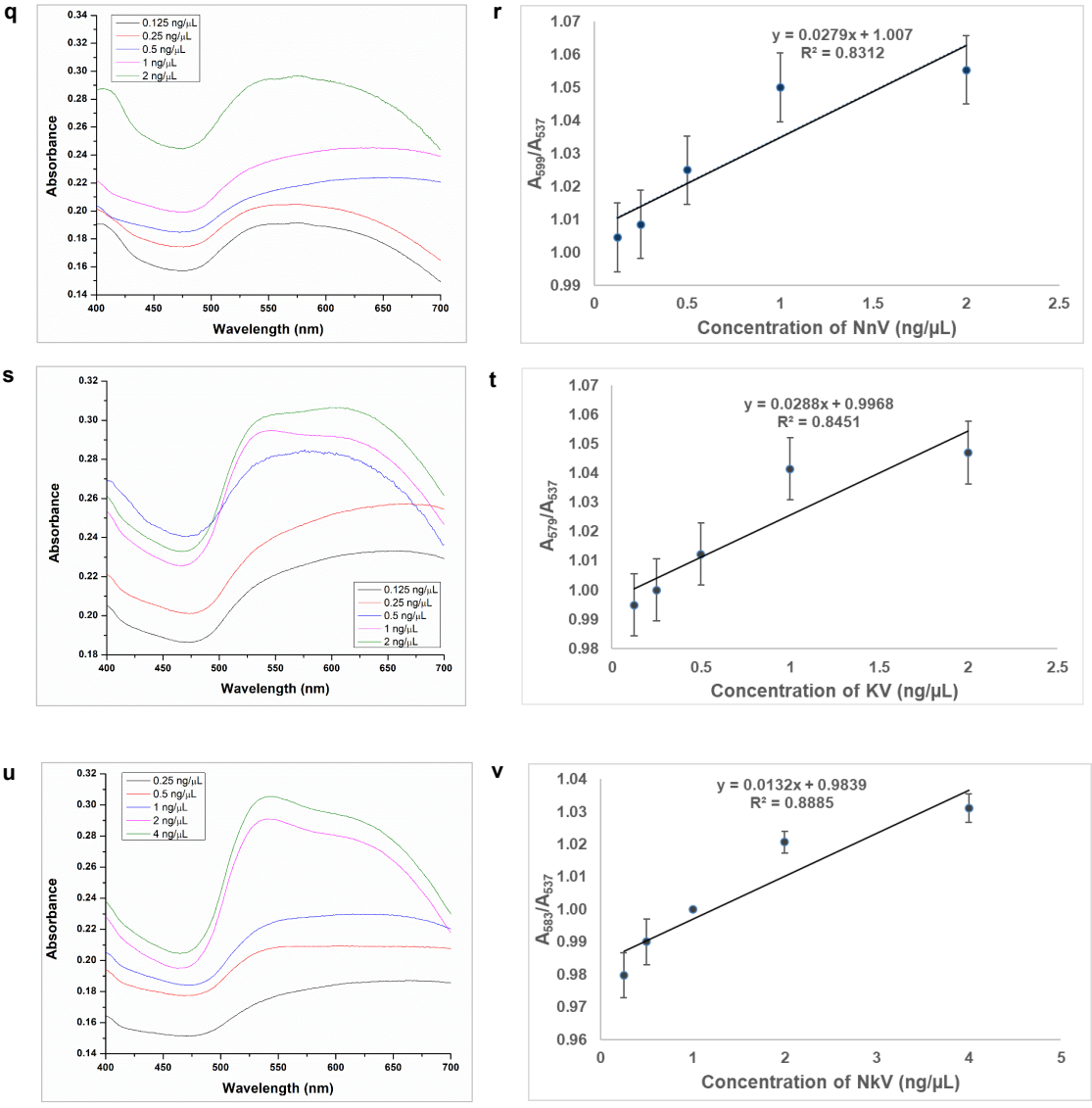

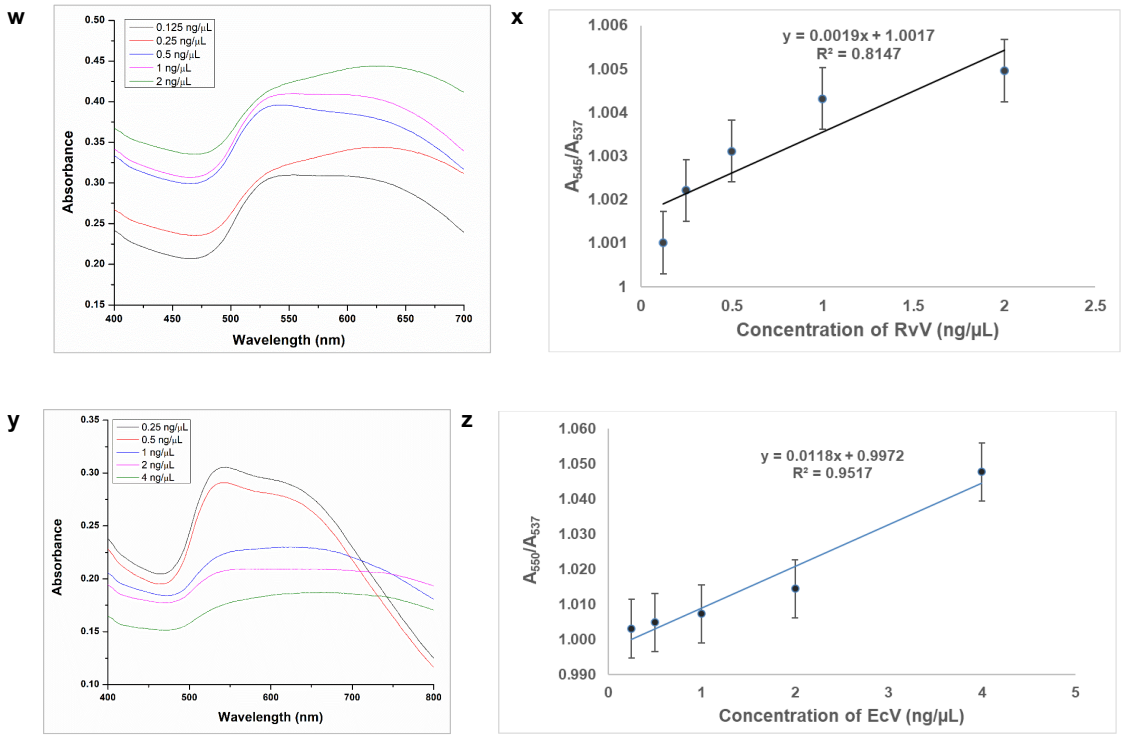

Fig 4.5 (q) Absorbance spectrum for NnV spiked rat plasma detection by AuNP-FPAb conjugate. Absorbance curves correspond to plasma samples containing 0.125-2 ng/µL NnV; **(r)** Calibration curve for NnV spiked rat plasma detection at concentrations 0.125-2 ng/µL; **(s)** Absorbance spectrum for KV spiked rat plasma detection by AuNP-FPAb conjugate. Absorbance curves correspond to plasma samples containing 0.125-2 ng/µL KV; **(t)** Calibration curve for KV spiked rat plasma detection at concentrations 0.125-2 ng/µL; **(u)** Absorbance spectrum for NkV spiked rat plasma detection by AuNP-FPAb conjugate. Absorbance curves correspond to plasma samples containing 0.25-4 ng/µL NkV; **(v)** Calibration curve for NkV spiked rat plasma detection at concentrations 0.25-4 ng/µL; **(w)** Absorbance spectrum for RvV spiked rat plasma detection by AuNP-FPAb conjugate. Absorbance curves correspond to plasma samples containing 0.125-2 ng/µL RvV; **(x)** Calibration curve for RvV spiked rat plasma detection at concentrations 0.125-2 ng/µL; **(y)** Absorbance spectrum for EcV spiked rat plasma detection by AuNP-FPAb conjugate. Absorbance curves correspond to plasma samples containing 0.25-4 ng/µL EcV; **(z)** Calibration curve for EcV spiked rat plasma detection at concentrations 0.25-4 ng/µL; Error bars indicate mean ± S.D. (n = 3).

Table 4.2 Determination of blue colour intensity and quantification of venom in envenomed rat plasma using Digital Image Colourimetry and UV-Vis spectrophotometer.

Plasma from rats envenomed with Indian snake venoms collection	**Time of blood collection (min)**	**Average I_B**	**Quantity of venom in plasma calculated using I_B (ng/µL)**	**Quantity of venom in plasma calculated using I_B (in percent of venom found in plasma)**	**Quantity of venom in plasma calculated using absorbance (ng/µL)**	**Quantity of venom in plasma calculated using absorbance (in percent of venom found in plasma)**
Indian cobra venom (NnV)	60	0.18	1.09	26.5	0.99	24.0
	120	0.17	1.01	24.6	0.68	16.5
	240	0.16	0.47	11.4	0.38	9.3
Indian krait venom (KV)	60	0.16	0.75	31.9	0.81	34.3
	120	0.16	0.65	27.7	0.70	29.9
	240	0.13	0.44	18.7	0.42	18
Indian monocled cobra venom (NkV)	60	0.19	1.85	22.5	2.46	29.9
	120	0.15	1.30	15.8	1.59	19.4
	240	0.14	1.11	13.5	1.48	18.0
Indian russell's viper venom (RvV)	60	0.21	2.07	50.4	2.35	57.4
	120	0.20	1.91	46.5	2.33	56.8
	240	0.19	1.81	44.0	2.24	54.2
Indian saw-scaled viper venom (EcV)	60	0.26	6.36	77.5	1.57	66.7
	120	0.24	5.74	70.0	1.47	62.6
	240	0.20	4.33	52.7	1.43	60.6

From Table 4.2, quantity of venom in envenomed plasma obtained from both digital image colourimetry and UV-Vis spectrophotometry was found to be comparable.

4.2 Discussion

Snakebite from a venomous snake may be either a 'wet bite' (venom injection) resulting in mild local symptoms to severe systemic toxicity and ultimately death, or they may be a 'dry bite' without local or systemic signs of envenomation [8-10]. Potential causes of 'dry bite' in various snake species may include a small amount of venom injection or no venom injection owing to the shape of the fangs and imprecise venom delivery [8]. Antivenom administration is the only current therapy for snakebite envenomation. However, this therapy has several adverse and costly effects [11]. Hence, using a method or kit to precisely determine whether a particular snakebite case is classified as a 'wet bite' or a 'dry bite' will significantly deter hospital authorities or physicians from delivering antivenom in every instance of snakebite [8].

This study describes the potential of a toxin-specific polyclonal antibody formulation to differentiate between bite cases with and without snake envenomation, commonly known as wet and dry snake bite, respectively, among India's medically critical venomous snakes. The produced polyclonal antibodies were combined in a specific ratio to create the antibody formulation FPAb, which exhibited synergistic immune recognition of the venoms under both *in vitro* and *in vivo* conditions. Detection of Indian snake venoms in envenomed rat plasma using the antibody formulation FPAb has been carried out using a digital image colourimetry method using AuNPs. Thus, this method may have potential to confirm venomous snakebites in samples for accurate diagnosis of envenomation.

Numerous researchers have employed various assays for developing tests or procedures for detecting snake envenomation from venomous snakes. In 2017, Shaikh et al. introduced the Venom Detection ELISA Test (VDET), a device utilizing dot-blot ELISA with plasma obtained from mice envenomed 60 minutes after venom injection. This test provides a binary result regarding envenomation by the Indian 'Big Four' venomous snakes and can be completed in 20-25 minutes, with a limit of detection of 1 ng/mL [12]. A recent study investigated the use of infrared thermal imaging to distinguish between venomous snakebites and non-venomous or dry bites in patients [13]. Most patients exhibiting signs of local envenomation, whether accompanied by systemic

envenomation or not, displayed temperature alterations. They obtained infrared photos in still image mode via a thermal imaging camera connected to an Android smartphone. The photos were subsequently analysed to ascertain the condition of envenomation [13]. Our work suggests a quick detection approach that may identify the presence of venom in plasma within 10 min, allowing us to distinguish between wet and dry snakebite cases. Furthermore, the antibody formulation described in our work demonstrated the detection of snake venoms in plasma up to 240 minutes after venom injection, which was not proven in the VDET trial. Though the LoD described in the current work is lower than the stated LoD of the VDET study, future investigations using monoclonal antibodies may boost the sensitivity of the current approach even further.

Additionally, two Indian patents for developing snake venom detection kits for Indian' Big Four' snake venoms have been granted [14,15]. The inventors of a specific patent have developed a method for producing monospecific antibodies, which exhibit no cross-reactivity with any of the other three species, and bispecific antibodies, which show no cross-reactivity with any of the other two species. This is an *in vitro* method that targets the Indian 'Big Four' snake venoms and includes the creation of lateral flow immunoassay devices that utilize the generated antibodies [15]. A separate patent introduced a two-site ELISA-based kit and a lateral flow immunoassay for detecting the venoms of the 'Big Four' Indian snakes in clinical samples from snakebite victims [14].

Toxins from families of PLA_2, snake venom metalloprotease, snake venom serine protease and three-finger toxins are generally dominant in the venom composition of all snake species [16]. Since developing a species-specific snake venom detection method necessitates targeting toxins from these families, there is a concern regarding a high degree of cross-reactivity between snake venom toxins of the same or heterologous family [1,10,17-19]. This reason has proven to be a hurdle in developing detection devices that may differentiate between genera/species of venomous snakes. Although numerous attempts have been put forward for detecting Indian snake venoms using various analytical methods like antigen-antibody interaction, aptamers, etc., one of them has been translated and commercialised for use in a clinical setting [12,14,15,20-22].

In recent years, the design and usage of synthetic peptides that mimic selected protein regions have seen a potential increase [23-27]. In this study, to circumvent the problem of using whole venom or purified venom-toxins as immunogens for the

production of polyclonal antibodies, we have synthesised custom peptide immunogens designed using the antigenic sites with the highest antigenic propensity from the major (high abundant) toxins like PLA_2 and snaclec of the Indian 'Big Four' venomous snakes. These antigenic sites were further modified to enhance their antigenic propensity, producing high antibody titre against these peptides. Generally, to raise high-titre polyclonal antibodies, it is necessary to conjugate the peptides to carrier protein such as KLH, bovine serum albumin (BSA), or ovalbumin [23,28,29]. Therefore, we conjugated the custom peptides with KLH in our study, ultimately producing high-titre polyclonal antibodies in rabbit serum.

The current study has used immunoblotting techniques to demonstrate the ability of toxin-specific antibody formulation, FPAb, to detect the presence of a picogram quantity of venom from Indian snakes in the body fluids of envenomed animals. Our study elucidates better immune recognition by FPAb than commercial (PAV) for Indian snake venoms at a low 1 pg/µL concentration under *in vitro* conditions. The observed effect may happen because FPAb comprises antibodies against the antigenic custom peptides designed explicitly from 'Big Four' snakes' low-molecular-mass toxins (PLA_2 and snaclec). On the contrary, the inferior immune recognition for the venoms by commercial PAV may be because they are raised against whole venom of the 'Big Four' snakes and they do not contain sufficient antibodies against the pharmacologically active, weakly immunogenic proteins of these venoms [30-35]. Given the ability of FPAb to detect the venom of 'Big Four' venomous snakes and *N. kaouthia,* under *in vitro* conditions, we have explored the potential of FPAb for detecting these venoms in animal plasma.

Animal models are crucial in experimental research (pre-clinical study) for refining diagnostic techniques and novel drug therapeutics before clinical trials [36]. In pharmacology and toxicology studies, experimental rats are generally preferred over mice as they share a similar toxin eradication pathway as humans [37]. Additionally, the larger body size of rats allows serial blood draws and sampling over time [38]. Therefore, our study has experimentally envenomed Wistar strain albino rats with the venoms of India's 'Big Four' venomous snakes and *N. kaouthia.* Compared to commercial PAV, FPAb better recognised the venom in plasma collected from the envenomed rats at regular intervals.

Generally, snakes envenom their victims by injecting their venoms mostly subcutaneously or occasionally intramuscularly, pending the release of the toxins into the interstitial space [39-41]. Studies have revealed that snake venom injected into patients gets absorbed quickly from the bloodstream, binding very rapidly with their target organs or specific receptors, thereby lessening the amount of venom left in systemic circulation for being detected by the diagnostic kit [10,42]. Snake venom in circulation may exhibit two phases: a quick distribution phase (within 60 min) and a prolonged elimination phase (12-24 h) [43-46]. Our study corroborates this observation, and we have demonstrated that immune recognition of the snake venoms in the envenomed plasma by FPAb decreased as time elapsed post-injection, i.e., venom detected in plasma at 240 min post-injection is lesser than at 60- and 120-min post-venom injections.

The interaction of venoms with AuNP-FPAb conjugates is known to cause agglomeration, which could give rise to a colour change. This characteristic of AuNP was utilised in this work to illustrate a colourimetric detection and quantification of the Indian Big Four poisonous snakes and *N. kaouthia* in envenomed rat plasma.

The formation of AuNPs and AuNP-FPAb bioconjugates was first confirmed using a few biophysical techniques. The size of the AuNP and AuNP-FPAb particles were determined to be about 18 nm and 37 nm, respectively, indicating the binding of antibodies to AuNP. It was observed that when envenomed plasmas from the rats were incubated with the AuNP-FPAb conjugates, colour of the solution changed from violet-pink to blue-grey colour within 5-10 min due to agglomeration [47,48]. Recent breakthroughs in the smartphone technology field have improved their usage to satisfy the needs of many scientific fields [49-51]. Thus, digital image colourimetry based on smartphone images could differentiate between control (non-envenomed) plasma and envenomed plasma and quantify the venom present in the envenomed plasma during the studied post-injection time duration. This method of detection technology will help detect envenomation in the health centres of remote villages where sophisticated instrumental facilities are not available. The venom quantity detected by FPAb in the plasma decreased as the time post-injection increased. Notably, since the antibodies constituting the FPAb were raised against antigenic peptides synthesised using the toxins of the 'Big Four' venomous snakes of India, it may have a lower affinity towards NkV and therefore, their detection in plasma may be lesser than the 'Big Four' snake venoms; though, sequence similarity observed between CP 1, CP 4 and *N. kaouthia* PLA_2 justify its venom detection

by the FPAb. An additional noteworthy finding was that the intensity of the blue colour in the plasma treated with Viperidae venoms (RvV and EcV) was greater than that in the plasma treated with Elapidae venom (NnV, KV, and NkV). Thus, more venom could be identified in the plasma of rats treated with Viperidae venom at a particular moment compared to those treated with Elapidae venom. The observed phenomenon can be attributed to the fast attachment of the Elapidae venoms, abundant in low molecular weight toxins, to their specific tissue targets. As a result, these venoms are promptly eliminated from the bloodstream. In contrast, Viperid venoms containing high-molecular-weight toxins are absorbed gradually from the injection site via the lymphatic system, resulting in prolonged and heightened presence in the bloodstream [41,52,53].

Snakebite cases are mostly occupational health hazard and affect rural population of the underdeveloped and developing countries [54]. Reports from India have suggested that majority of the snakebite deaths have been recorded in rural areas (97%) during monsoon months [54]. However, the unofficial count of morbidity and mortality due to snake envenomation may be far higher due to poor documentation [10]. In clinical settings, it is crucial to determine whether a snakebite is wet or dry since this knowledge informs the right medical actions, such as deciding whether antivenom is required. [55]. The World Health Organization (WHO) has stated that snakebite management mainly relies on identifying snake species, clinical diagnosis, and the appropriate administration of antivenoms. The WHO recommendations emphasize the necessity for commercial tests that confirm snake envenomation, enabling doctors to select and deliver the optimum amount of antivenoms for patient treatment [56]. This study proposes a portable smartphone-based colourimetric method for detecting and quantifying venom from the Indian 'Big Four' snakes, which is essential for antivenom therapy, potentially leading to developing a device for on-site assessment of envenomation in patients. The snake envenomation detection approach presented in this paper may enable medical professionals to ascertain if a snakebite is venomous or non-venomous, enhancing hospital care of snake envenomation cases. Nevertheless, other constraints must be resolved before using this technology in a clinical context. The current detection approach necessitates clinical testing using bodily fluid samples from victims of snake envenomation. The clinical study must incorporate an adequate sample size of actual victim samples to validate the applicability of the FPAb for detection purposes in clinical settings. Since the proposed method is a proof-of-concept, future investigations may be

designed to refine antibody raising, and monoclonal antibodies raised against the snake venom toxins may be considered to develop a particular and sensitive detection method. Furthermore, the concurrent binding of two antibody molecules to one or two PLA_2/snaclec may be impractical due to steric hindrance, particularly on the solid membrane surface. Since the identical formulation has been utilized for both capture and primary antibodies, certain epitopes on the captured PLA_2/snaclec may be obstructed by the antibody fixed on the membrane. Consequently, the homologous binding of the primary antibodies to PLA_2/snaclec may be suboptimal and non-stoichiometric. Consequently, additional experiments are necessary to enhance the antigen-antibody binding for improved immune recognition sensitivity. Furthermore, the smartphone-based detection system presented in this work requires improvements in real-time result processing, interpretation, and communication to necessary staff before it can be used in rural clinics.

This study presents a straightforward and cost-effective method that could aid in developing kits for treating venomous snakebites in patients. The research indicates the generation of polyclonal antibodies targeting toxins from India's four most venomous snakes. The antibodies generated were combined in a specific ratio to illustrate synergistic immune recognition of India's 'Big Four' venomous snakes and *N. kaouthia* venoms both *in vitro* and *in vivo*. Digital image colourimetry enhanced the detection of the antibody formulation. Further research is necessary to validate the suitability of this detection method using envenomed patient plasma and other body fluids in both field and clinical settings. Given that data from the diagnostic test may also benefit retrospective epidemiological studies on envenomation episodes, subsequent research may encompass snakes beyond the 'Big Four' and *N. kaouthia*. These new kits may identify venoms that the existing antivenom can neutralize. In instances of envenomation lacking a particular antivenom, accessible antivenom may be administered to preserve the patient's life, owing to the potential para-specificity of the antivenom. In these instances, a diagnostic kit may prove beneficial in assessing therapy efficacy by identifying trace venom in the patient's systemic circulation, thereby clarifying the cross-reactivity of the available antivenom with the identified venom. Consequently, data acquired via diagnostics may prove invaluable in understanding the incidence of bites from snakes beyond the 'Big Four,' thereby informing the development of future antivenoms to address snakebite cases in India comprehensively.

Bibliography:

[1] Kakati, H., Patra, A., Kalita, B., Chanda, A., Rapole, S., and Mukherjee, A. K. A comparison of two different analytical workflows to determine the venom proteome composition of *Naja kaouthia* from North-East India and immunological profiling of venom against commercial antivenoms. *Int. J. Biol. Macromol.*, 208: 275-287, 2022.

[2] Frens, G. Controlled nucleation for the regulation of the particle size in monodisperse gold suspensions. *Nat. Phys. Sci.*, 241(105): 20-22, 1973.

[3] Kimling, J., Maier, M., Okenve, B., Kotaidis, V., Ballot, H., and Plech, A. Turkevich method for gold nanoparticle synthesis revisited. *J. Phys. Chem. B*, 110(32): 15700-15707, 2006.

[4] Herizchi, R., Abbasi, E., Milani, M., and Akbarzadeh, A. Current methods for synthesis of gold nanoparticles. *Artif. Cells Nanomed. Biotechnol*, 44(2): 596-602, 2016.

[5] Stuart, B. H. *Infrared spectroscopy: fundamentals and applications*. John Wiley & Sons, England, 1-221, 2004.

[6] Firdaus, M. L., Alwi, W., Trinoveldi, F., Rahayu, I., Rahmidar, L., and Warsito, K. Determination of chromium and iron using digital image-based colorimetry. *Procedia Environ. Sci.*, 20: 298-304, 2014.

[7] Aqillah, F., Permana, M. D., Eddy, D. R., Firdaus, M. L., Takei, T., and Rahayu, I. Detection and quantification of Cu2+ ion using gold nanoparticles via Smartphone-based digital imaging colorimetry technique. *Results Chem*, 7: 101418, 2024.

[8] Naik, B. S. “Dry bite” in venomous snakes: A review. *Toxicon*, 133: 63-67, 2017.

[9] Warrell, D. A. *Guidelines for the management of snake-bites*. World Health Organization, Geneva, 1-162, 2010.

[10] Puzari, U. and Mukherjee, A. K. Recent developments in diagnostic tools and bioanalytical methods for analysis of snake venom: A critical review. *Anal Chim Acta*, 1137: 208-224, 2020.

[11] Puzari, U., Fernandes, P. A., and Mukherjee, A. K. Advances in the therapeutic application of small-molecule inhibitors and repurposed drugs against snakebite: Miniperspective. *J Med Chem*, 64(19): 13938-13979, 2021.

[12] Shaikh, I. K., Dixit, P. P., Pawade, B. S., and Waykar, I. G. Development of dot-ELISA for the detection of venoms of major Indian venomous snakes. *Toxicon*, 139: 66-73, 2017.

[13] Sabitha, P., Bammigatti, C., Deepanjali, S., Suryanarayana, B. S., and Kadhiravan, T. Point-of-care infrared thermal imaging for differentiating venomous snakebites from non-venomous and dry bites. *PLoS Negl Trop Dis*, 15(2): e0008580, 2021.

[14] Vaiyapuri, R. and Williams, H. F. METHODS, COMPOSITIONS AND KITS FOR VENOM DETECTION. India patent (2019).

[15] Lorven, B. SNAKE VENOM DETECTION KIT. India patent (2018).

[16] Tasoulis, T. and Isbister, G. K. A current perspective on snake venom composition and constituent protein families. *Arch. Toxicol.*, 97(1): 133-153, 2023.

[17] Ratanabanangkoon, K., Tan, K. Y., Pruksaphon, K., Klinpayom, C., Gutiérrez, J. M., Quraishi, N. H., and Tan, C. H. A pan-specific antiserum produced by a novel immunization strategy shows a high spectrum of neutralization against neurotoxic snake venoms. *Sci Rep*, 10(1): 11261, 2020.

[18] Ainsworth, S., Slagboom, J., Alomran, N., Pla, D., Alhamdi, Y., King, S. I., Bolton, F. M., Gutiérrez, J. M., Vonk, F. J., and Toh, C.-H. The paraspecific neutralisation of snake venom induced coagulopathy by antivenoms. *Comm Biol* 1(1): 34, 2018.

[19] Tan, C. H., Liew, J. L., Tan, N. H., Ismail, A. K., Maharani, T., Khomvilai, S., and Sitprija, V. Cross reactivity and lethality neutralization of venoms of Indonesian *Trimeresurus* complex species by Thai Green Pit Viper Antivenom. *Toxicon*, 140: 32-37, 2017.

[20] Kaul, S., Sai Keerthana, L., Kumar, P., Birader, K., Tammineni, Y., Rawat, D., and Suman, P. Cytotoxin antibody-based colourimetric sensor for field-level differential detection of elapid among big four snake venom. *PLoS Negl Trop Dis*, 15(10): e0009841, 2021.

[21] Ramana, L. N., Mathapati, S. S., Salvi, N., Khadilkar, M., Malhotra, A., Santra, V., and Sharma, T. K. A paper microfluidic device based colorimetric sensor for the detection and discrimination of elapid versus viper envenomation. *Analyst*, 147(4): 685-694, 2022.

[22] Selvanayagam, Z. E., Gnanavendhan, S., Ganesh, K., Rajagopal, D., and Rao, P. S. ELISA for the detection of venoms from four medically important snakes of India. *Toxicon*, 37(5): 757-770, 1999.

[23] Trier, N. H., Hansen, P., and Houen, G. Production and characterization of peptide antibodies. *Methods*, 56(2): 136-144, 2012.

[24] Lee, B.-S., Huang, J.-S., Jayathilaka, L. P., Lee, J., and Gupta, S. Antibody production with synthetic peptides. In S Schwartzbach, Skalli, O, Schikorski, T, *Methods*

in Molecular Biology 1474 of, pages 25-47, 1493963503. Humana Press, New York, NY, 2016.

[25] Trier, N., Hansen, P., and Houen, G. Peptides, antibodies, peptide antibodies and more. *Int J Mol Sci*, 20(24): 6289, 2019.

[26] Madhubala, D., Patra, A., Islam, T., Saikia, K., Khan, M. R., Ahmed, S. A., Borah, J. C., and Mukherjee, A. K. Snake venom nerve growth factor-inspired designing of novel peptide therapeutics for the prevention of paraquat-induced apoptosis, neurodegeneration, and alteration of metabolic pathway genes in the rat pheochromocytoma PC-12 cell. *Free Radic Biol Med*, 197: 23-45, 2023.

[27] Puzari, U., Khan, M. R., and Mukherjee, A. K. Development of a gold nanoparticle-based novel diagnostic prototype for *in vivo* detection of Indian red scorpion (*Mesobuthus tamulus*) venom. *Toxicon: X*: 100203, 2024.

[28] Schaaper, W., Lankhof, H., Puijk, W., and Meloen, R. Manipulation of antipeptide immune response by varying the coupling of the peptide with the carrier protein. *Mol Immunol*, 26(1): 81-85, 1989.

[29] Houen, G., Olsen, D., Hansen, P., Petersen, K., and Barkholt, V. Preparation of bioconjugates by solid-phase conjugation to ion exchange matrix-adsorbed carrier proteins. *Bioconj Chem*, 14(1): 75-79, 2003.

[30] Kalita, B., Patra, A., and Mukherjee, A. K. Unraveling the proteome composition and immuno-profiling of western India Russell's viper venom for in-depth understanding of its pharmacological properties, clinical manifestations, and effective antivenom treatment. *J. Proteome Res.* , 16(2): 583-598, 2017.

[31] Chanda, A. and Mukherjee, A. K. Quantitative proteomics to reveal the composition of Southern India spectacled cobra (*Naja naja*) venom and its immunological cross-reactivity towards commercial antivenom. *International Journal of Biological Macromolecules*, 160: 224-232, 2020.

[32] Patra, A., Chanda, A., and Mukherjee, A. K. Quantitative proteomic analysis of venom from Southern India common krait (*Bungarus caeruleus)* and identification of poorly immunogenic toxins by immune-profiling against commercial antivenom. *Expert review of proteomics*, 16(5): 457-469, 2019.

[33] Patra, A., Kalita, B., Chanda, A., and Mukherjee, A. K. Proteomics and antivenomics of *Echis carinatus carinatus* venom: Correlation with pharmacological properties and pathophysiology of envenomation. *Scientific reports*, 7(1): 17119, 2017.

[34] Deka, A., Bhatia, S., Santra, V., Bharti, O. K., Lalremsanga, H. T., Martin, G., Wüster, W., Owens, J. B., Graham, S., and Doley, R. Multilevel comparison of Indian *Naja* venoms and their cross-reactivity with Indian polyvalent antivenoms. *Toxins*, 15(4): 258, 2023.

[35] Laxme, R. S., Khochare, S., de Souza, H. F., Ahuja, B., Suranse, V., Martin, G., Whitaker, R., and Sunagar, K. Beyond the 'big four': Venom profiling of the medically important yet neglected Indian snakes reveals disturbing antivenom deficiencies. *PLoS Negl Trop Dis*, 13(12): e0007899, 2019.

[36] Domínguez-Oliva, A., Hernández-Ávalos, I., Martínez-Burnes, J., Olmos-Hernández, A., Verduzco-Mendoza, A., and Mota-Rojas, D. The importance of animal models in biomedical research: current insights and applications. *Animals*, 13(7): 1223, 2023.

[37] Huang, G., Ashton, C., Kumbhani, D. S., and Ying, Q.-L. Genetic manipulations in the rat: progress and prospects. *Curr Opin Nephrol Hypertens*, 20(4): 391-399, 2011.

[38] Hashway, S. A. and Wilding, L. A. Translational potential of rats in research. In Mark A. Suckow, F. Claire Hankenson, Ronald P. Wilson, & Patricia L. Foley, *The laboratory rat*, of, pages 77-88. Elsevier, 2020.

[39] Anai, K., Sugiki, M., Yoshida, E., and Maruyama, M. Neutralization of a snake venom hemorrhagic metalloproteinase prevents coagulopathy after subcutaneous injection of *Bothrops jararaca* venom in rats. *Toxicon*, 40(1): 63-68, 2002.

[40] Gutiérrez, J. M., Calvete, J. J., Habib, A. G., Harrison, R. A., Williams, D. J., and Warrell, D. A. Snakebite envenoming. *Nat. Rev. Dis. Primers*, 3(1): 1-21, 2017.

[41] Paniagua, D., Vergara, I., Boyer, L., and Alagón, A. Role of lymphatic system on snake venom absorption. In Hidetoshi Inagaki P. Gopalakrishnakone, Carl-Wilhelm Vogel, Ashis K. Mukherjee, Tarek R. Rahmy, *Snake Venoms*, of, pages 453-474. Springer, Dordrecht: Springer Netherlands, 2017.

[42] Hung, D.-Z., Liau, M.-Y., and Lin-Shiau, S.-Y. The clinical significance of venom detection in patients of cobra snakebite. *Toxicon*, 41(4): 409-415, 2003.

[43] Yap, M. K. K., Tan, N. H., Sim, S. M., Fung, S. Y., and Tan, C. H. Pharmacokinetics of *Naja sumatrana* (equatorial spitting cobra) venom and its major toxins in experimentally envenomed rabbits. *PLoS Negl Trop Dis*, 8(6): e2890, 2014.

[44] Sanhajariya, S., Duffull, S. B., and Isbister, G. K. Pharmacokinetics of snake venom. *Toxins*, 10(2): 73, 2018.

[45] Guo, M.-P., Wang, Q.-C., and Liu, G.-F. Pharmacokinetics of cytotoxin from Chinese cobra (*Naja naja atra*) venom. *Toxicon*, 31(3): 339-343, 1993.

[46] Choowongkomon, K., Chaisakul, J., Seetaha, S., Vasaruchapong, T., Hodgson, W. C., Rasri, N., Chaeksin, K., Boonchaleaw, S., and Sookprasert, N. Development of a biosensor to detect venom of Malayan krait (*Bungarus candidus*). *Toxins*, 16(1): 56, 2024.

[47] Ngernpimai, S., Srijampa, S., Thongmee, P., Teerasong, S., Puangmali, T., Maleewong, W., Chompoosor, A., and Tippayawat, P. Insight into the covalently oriented immobilization of antibodies on gold nanoparticle probes to improve sensitivity in the colorimetric detection of listeria monocytogenes. *Bioconj Chem*, 33(11): 2103-2112, 2022.

[48] Bastos-Soares, E. A., da Silva Morais, M. S., Funes-Huacca, M., Sousa, R. M. O., Brilhante-Da-Silva, N., Roberto, S. A., Prado, N. D. R., Dos Santos, C. N. D., Marinho, A. C., and Soares, A. M. Single-Domain Antibody-Gold Nanoparticle Bioconjugates as Immunosensors for the Detection of Hantaviruses. *Mol Diag Ther*: 1-16, 2024.

[49] Potluri, V., Kathiresan, P. S., Kandula, H., Thirumalaraju, P., Kanakasabapathy, M. K., Pavan, S. K. S., Yarravarapu, D., Soundararajan, A., Baskar, K., and Gupta, R. An inexpensive smartphone-based device for point-of-care ovulation testing. *Lab on a Chip*, 19(1): 59-67, 2019.

[50] Tong, H., Cao, C., You, M., Han, S., Liu, Z., Xiao, Y., He, W., Liu, C., Peng, P., and Xue, Z. Artificial intelligence-assisted colorimetric lateral flow immunoassay for sensitive and quantitative detection of COVID-19 neutralizing antibody. *Biosens and Bioelectron*, 213: 114449, 2022.

[51] Solra, M., Das, S., and Rana, S. Point-of-care detection of hydroxyurea drug in serum using a supramolecular enzyme mimetic. *Sens Actuators B Chem*, 406: 135424, 2024.

[52] Slagboom, J., Kool, J., Harrison, R. A., and Casewell, N. R. Haemotoxic snake venoms: their functional activity, impact on snakebite victims and pharmaceutical promise. *Br J Haematol*, 177(6): 947-959, 2017.

[53] Gamulin, E., Mateljak Lukačević, S., Halassy, B., and Kurtović, T. Snake Antivenoms—Toward Better Understanding of the Administration Route. *Toxins*, 15(6): 398, 2023.

[54] Mohapatra, B., Warrell, D. A., Suraweera, W., Bhatia, P., Dhingra, N., Jotkar, R. M., Rodriguez, P. S., Mishra, K., Whitaker, R., and Jha, P. Snakebite mortality in India: a nationally representative mortality survey. *PLoS Negl Trop Dis*, 5(4): e1018, 2011.

[55] Pucca, M. B., Knudsen, C., S. Oliveira, I., Rimbault, C., A. Cerni, F., Wen, F. H., Sachett, J., Sartim, M. A., Laustsen, A. H., and Monteiro, W. M. Current knowledge on snake dry bites. *Toxins*, 12(11): 668, 2020.

[56] Organization, W. H. Guidelines for the clinical management of snake bites in the South-East Asia Region. Technical Report, New Delhi WHO South East Asia Regional Office, 2005.